


<https://doi.org/10.1038/s42003-024-07312-0>

Concomitant loss of TET2 and TET3 results in T cell expansion and genomic instability in mice



Marianthi Gioulbasani^{1,2,6}, Tarmo Äijö^{1,6}, Siyao Liu¹, Stephanie A. Montgomery^{1,3}, Nathan D. Montgomery^{1,3}, David Corcoran^{1,4} & Ageliki Tsagaratou ^{1,4,5} ✉

Ten eleven translocation (TET) proteins are tumor suppressors that through their catalytic activity oxidize 5-methylcytosine to 5-hydroxymethylcytosine, to promote DNA demethylation and to regulate gene expression. Notably, TET2 is one of the most frequently mutated genes in hematological malignancies, including T cell lymphomas. However, murine models with deletion of TET2 do not exhibit T cell expansion, presumably due to redundancy with other members of the TET family of proteins. In order to gain insight on the TET mediated molecular events that safeguard T cells from aberrant proliferation we performed serial adoptive transfers of murine CD4 T cells that lack concomitantly TET2 and TET3 to fully immunocompetent congenic mice. Here we show a progressive acquisition of malignant traits upon loss of TET2 and TET3 that is characterized by loss of genomic integrity, acquisition of aneuploidy and upregulation of the protooncogene *Myc*.

TET proteins are Fe²⁺ and O₂ dependent deoxygenases. There are three TET proteins; TET1, TET2 and TET3. They are characterized by a common, evolutionary conserved carboxyl-terminal catalytic domain that mediates oxidization of 5-methylcytosine (5mC) to 5-hydroxymethylcytosine (5hmC)¹ and other oxidized cytosines (oxi-mCs), namely 5-formylcytosine (5fC) and 5-carboxylcytosine (5caC)². Importantly, loss of 5hmC correlates with myelodysplastic syndromes³. TET2 is one of the most frequently mutated genes in hematological cancers^{4–6}, including angioimmunoblastic T cell lymphoma (AITL)^{7–9} and peripheral T cell lymphoma, non-otherwise specified (PTCL-NOS)¹⁰. It has been suggested that TET2 mutations are an early event during the process of malignant transformation and confer proliferative advantage to the mutant cells^{4,6,10}. Deletion of TET2 in mouse models confers proliferative advantage in hematopoietic stem cells (HSCs) in vivo and enhanced proliferation in serial plating assays^{11,12} in a catalytic dependent manner^{13,14}. However, exclusive deletion of TET2 in murine models is not sufficient to result in T cell expansion, presumably due to redundant functions with other TET proteins. In addition, it has been demonstrated that TCR-mediated activation of T cells that lack Tet2 and have a point mutation of RhoAG17V contributes to the hyperproliferation of the cells, resulting in AITL¹⁵. RhoAG17V is a dominant negative mutant that inhibits RHO signaling⁹. Notably, deletion of TET2 was instrumental for

the proliferation of the cells but the point mutation of RhoA drove the acquisition of the follicular T helper (T_{fh}) phenotype¹⁵.

It is not clear how loss of TET proteins might contribute to the expansion of T cells. We have previously demonstrated that 5hmC is dynamically distributed across the genome of developing T cells¹⁶. We have shown that TET3 can interact with proteins involved in RNA splicing, transcriptional elongation, chromatin conformation and DNA repair¹⁷. In addition, we have analyzed the impact of TET loss in T cell development in vivo^{18,19}. Our data revealed an expansion of invariant natural killer (iNKT) cells and increased representation of the NKT17 lineage that is defined by the lineage specifying factor ROR γ t^{18,19}. Mechanistically, the upregulation of ROR γ t was attributed to the concomitant downregulation of the transcription factors Tbet and ThPOK that gained methylation upon TET2 and TET3 loss. In addition, we showed that TET2 and TET3 regulate *Drosha* expression in thymic iNKT and thymic CD4 single positive cells²⁰, potentially impacting expression of small RNAs. Interestingly, small RNA-seq comparing thymic control and *Tet2/3* DKO iNKT cells revealed downregulation of small RNAs including Let-7 microRNAs that were shown to downregulate PLZF expression^{20,21}. Collectively, our discoveries shed light in the TET-mediated regulation of T cell lineage specification. However, we were not able to identify a specific molecular mechanism that would explain the expansion of *Tet2/3* DKO iNKT cells. Notably, the whole genome

¹Lineberger Comprehensive Cancer Center, University of North Carolina at Chapel Hill, Chapel Hill, NC, USA. ²School of Biology, Aristotle University of Thessaloniki, 54124 Thessaloniki, Greece. ³Department of Pathology and Laboratory Medicine, University of North Carolina at Chapel Hill, Chapel Hill, USA.

⁴Department of Genetics, University of North Carolina at Chapel Hill, Chapel Hill, NC, USA. ⁵Department of Microbiology and Immunology, University of North Carolina at Chapel Hill, Chapel Hill, NC, USA. ⁶These authors contributed equally: Marianthi Gioulbasani, Tarmo Äijö. ✉e-mail: ageliki_tsagaratou@med.unc.edu

bisulfite sequencing (WGBS) datasets that we generated to evaluate differences in DNA methylation revealed a limited number of changes in global DNA methylation upon TET2 and TET3 loss, suggesting a focal action of TET proteins in the process of DNA demethylation¹⁸.

In addition, numerous groups have demonstrated a critical role for TET proteins in regulating the stability of regulatory T (Treg) cell lineage^{22–24} consistent with a gradual loss of Tregs in *Tet2/3* DKO mice. In the periphery, we observed a striking reduction of *Tet2/3* DKO CD8 cells, precluding additional characterization of these cells in vivo. The mutant mice died around 7 weeks old. Due to the accelerated death it was not possible to dissect whether loss of TET proteins might impact CD4 T cell expansion^{18,22}.

In this report, we aimed to decipher the impact of TET proteins in controlling in vivo proliferation of peripheral T cells. We employed adoptive transfer of *Tet2/3* DKO T cells and we discovered that *Tet2/3* DKO CD4 cells exhibited upregulation of genes involved in proliferation upon serial transplantation. This altered gene expression program endowed *Tet2/3* DKO CD4 cells with increased proliferative capacity and acquisition of malignant traits, such as expansion and chromosomal copy number (CCN) variations, resulting in aggressive lymphoproliferative disorders. In addition, we demonstrated that as the TET deficient cells acquired a hyper-proliferative profile they could expand remarkably fast, within 10 days, in recipient mice. During this rapid expansion of transplanted *Tet2/3* DKO T cells, by employing an unbiased, single cell transcriptomic approach, we revealed that while the immune environment of the host mice became rapidly activated, it failed to annihilate the expansion of the donor T cells.

Results

Tet2/3 DKO T cells exhibit increased proliferation

In order to understand what are the changes that occur in the gene expression program of *Tet2/3* deficient CD4 T cells, we isolated cells by FACS sorting (Supplementary Fig. 1) from young mice (ranging from 22 to 27 days old) to avoid the lymphoproliferative diseases previously described for these mice as they grow older^{18,22}. Indeed, at this age, the total cell number of the isolated spleens was comparable (Fig. 1a). As control, we used CD4 cells from wild type sex and age matched mice (Supplementary Fig. 2). The sorted *Tet2/3* DKO CD4 cells consist of the total population of CD4 cells: naïve, memory and effector CD4+ T cells excluding CD25+ cells that represent Tregs and aGalCer⁺ TCRβ intermediate cells that represent iNKT cells²⁵ (Supplementary Fig. 1). We opted to exclude iNKT cells since we have previously demonstrated that *Tet2/3* DKO iNKT cells exhibit lymphoproliferative traits upon transplantation to congenic mice¹⁸. In addition, we chose to exclude *Tet2/3* DKO Tregs since the impact of TET proteins on this population has been extensively characterized and thus it was out of the scope of the present study^{22,23}. The sorted *Tet2/3* DKO cells had a purity of 95% (Supplementary Fig. 1). As expected the vast majority of the control CD4 cells were naïve, expressing CD62L and lacking expression of the CD44 activation marker (Fig. 1b). The *Tet2/3* DKO CD4 cells isolated from mice shortly after weaning were mainly naïve (Fig. 1b). However, even at this young age we noticed a significant reduction of *Tet2/3* DKO naïve CD4 cells and an increase of the activated CD44+CD62L+ as well as CD44+CD62L– cells, reflecting the acquisition of activation (Fig. 1b, c).

Our unbiased transcriptomic analysis revealed 3560 differentially expressed genes (DEGs), among which 1478 were downregulated and 2,082 were upregulated (Fig. 1d and Supplementary Fig. 3). Given the established role of TET proteins as DNA demethylases the increased number of upregulated genes may appear paradoxical. However, this is a common finding in TET deficient cells, including immune cells such as iNKT cells¹⁸, Tregs²⁶, B cells²⁷, HSCs²⁸. Importantly, we identified upregulation of genes encoding for transcription factors that play critical roles in lineage specification such as *Rorc*, as well as genes such as the proliferation marker *Mki67* (also known as *Ki67*) that overall suggest an increased proliferative potential. We did not detect upregulation of *Gata3* or the cytokine IL-4. We also confirmed that there was no differential expression of *Cd4* (Fig. 1d). In addition, we noticed upregulation of *Hes1* even though the adjusted *p* value was 0.012, slightly less than the cutoff *p* value for statistical significance that

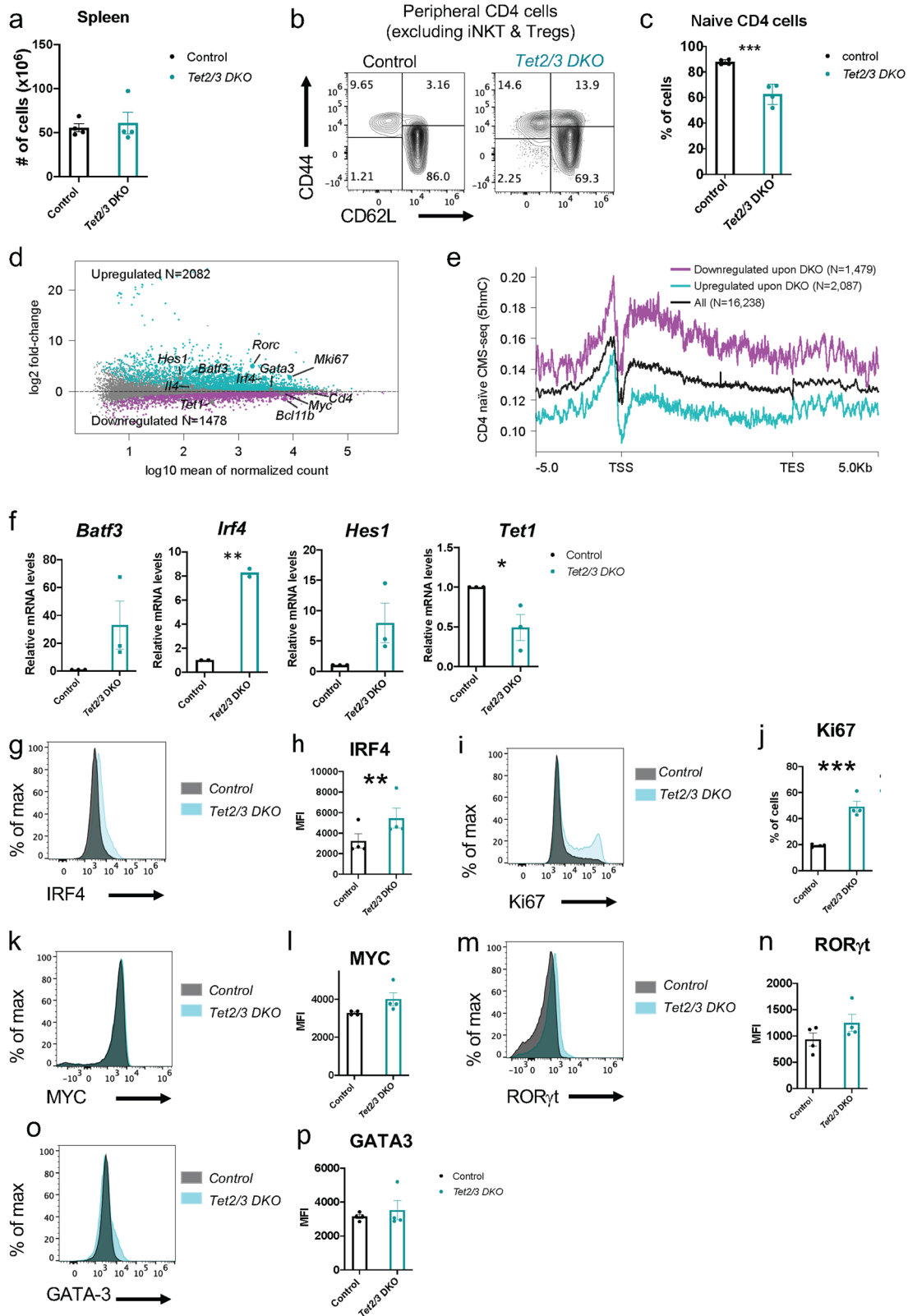
we set at 0.01 (Fig. 1d). *Hes1* is a Notch target gene that has been implicated in T cell leukemias and lymphomas^{29,30}. Finally, we identified upregulation of genes that encode for critical transcription factors such as *Batf3* and *Irf4* (Fig. 1d). BATF3 and IRF4 upregulation has been reported in T cell lymphomas and was suggested to induce *Myc* upregulation³¹. However, we did not detect the protooncogene *Myc* among the DEGs (Fig. 1d). Interestingly, among the downregulated genes we detected *Tet1* with adjusted *p* value 0.0119, which is slightly less than our statistically significant adjusted *p* value 0.01 (Fig. 1d). Reduced *Tet1* expression could be potentially due to impairment of TET2 and TET3 mediated de-methylation and induction of TET1 expression. Importantly, the upregulation of numerous transcription factors can explain, at least to some extent, how loss of TET proteins not only results in down-regulation of genes but also in a significant upregulation of numerous genes (Fig. 1d). Among the downregulated genes, we identified genes important for T cell biology, such as *Bcl11b* (Fig. 1d), that we have previously identified to be enriched for 5hmC in T cell subsets^{16,18,19}.

TET proteins through their catalytic activity oxidize 5mC to 5hmC¹. Thus, we wondered how 5hmC distribution correlated to the DEGs that we identified (Fig. 1d). To this end, we investigated the distribution of 5hmC, leveraging our previously published cytosine-5-methylenesulfonate (CMS)³²-IP-seq^{33,34} datasets¹⁶ in naïve wild type CD4 cells, which constitute the vast majority of the total CD4 cells (Fig. 1b, c). Our analysis indicated that downregulated genes in *Tet2/3* DKO total CD4 cells (Fig. 1e, Supplementary Data 1) have more intragenic 5hmC in wild type CD4 cells, compared to genes that are upregulated upon TET loss and compared to all genes (Fig. 1e, Supplementary Data 1). Interestingly, genes that are upregulated in *Tet2/3* DKO T cells have less intragenic 5hmC in the WT CD4 cells compared to downregulated and all genes. Overall, these trends agree with the positive correlation of intragenic 5hmC with gene expression that we and others have previously reported in T cells^{16,35–37}.

Next, we focused on specific genes of interest and we followed up either by quantitative polymerase chain reaction (qPCR) or/ and by flow cytometry experiments in order to confirm their altered expression. Specifically, we confirmed by qPCR the upregulation of *Batf3*, *Irf4*, *Hes1* and the downregulation of *Tet1* (Fig. 1f). We clarify that the statistical analysis we performed (unpaired *t* test) confirmed statistical significance for *Irf4* and *Tet1* expression. For additional genes of interest, for which there were available antibodies, we focused on protein expression and we assessed this by flow cytometry. We confirmed at the protein level that *Tet2/3* DKO CD4 cells upregulate the transcription factor IRF4 (Fig. 1g, h). Our data confirmed that there were more Ki67 positive *Tet2/3* DKO CD4 cells compared to the wild type CD4 cells (Fig. 1i, j), indicating an increased proliferative potential of the *Tet2/3* DKO CD4 cells. We were not able to find an antibody to detect BATF3 in murine samples. However, as IRF4 and BATF3 are important for upregulation of MYC^{31,38} we evaluated protein levels of MYC in our samples (Fig. 1k–l). Our flow cytometry data agreed with the RNA-seq data, indicating similar levels of MYC among control and *Tet2/3* DKO CD4 cells. Finally, we focused on key transcription factors for T cell differentiation. While *Rorc* was detected among the upregulated genes (Fig. 1d) we observed only a small increase at the protein level, which however was not statistically significant (Fig. 1m, n). We also evaluated GATA3 protein levels in our samples. Similar to the RNA-seq data we did not detect statistically significant difference for this transcription factor in our samples (Fig. 1o, p). Collectively, *Tet2/3* DKO CD4 T cells exhibit increased proliferation.

Tet2/3 DKO T cells manifest lymphoproliferative expansion upon serial transplantations

We previously published that *Tet2/3* DKO mice die at a young age (around 7–8 weeks old)¹⁸. Thus, it was not possible to assess how the *Tet2/3* DKO CD4 T cells would behave in the course of time. In addition, *Tet2/3* DKO Tregs progressively lose *Foxp3* expression due to methylation of the CNS2 locus that is critical for the stable expression of this factor²². Ultimately, the *Tet2/3* DKO Tregs are not functional and cannot suppress the proliferation of *Tet2/3* DKO T cells. An additional defect is the expansion of *Tet2/3* DKO



iNKT cells with NKT17 properties that secrete large amounts of IL-17, contributing further to the activation of the *Tet2/3* DKO CD4 cells¹⁸. To test whether loss of TET2 and TET3 could endow *Tet2/3* DKO CD4 cells with hyperproliferative capacity that cannot be suppressed by functional, wild type Tregs we performed serial transplantations of sorted, highly pure

Tet2/3 DKO CD4 cells (Supplementary Fig. 1) in congenic CD45.1⁺ recipients, that did not receive any irradiation (Fig. 2a).

After 16 weeks, we witnessed that the transferred CD45.2⁺ *Tet2/3* DKO cells evaded the immune surveillance of the recipients and expanded. The phenotypic analysis of the first transplantation revealed that the recipient

Fig. 1 | Characterization of *Tet2/3* DKO CD4 T cells. **a** Spleens were isolated from control and *Tet2/3* DKO mice at 25 days old. Spleens were dissociated to obtain single cell suspensions and total cell numbers were counted. No statistical significance was detected by unpaired Student's *t* test. Each dot in the graph represents a mouse. The bar graph represents the mean \pm standard error (SEM). **b** Single cell suspensions from spleens of control and *Tet2/3* DKO mice were prepared. Cells were stained with fluorescent conjugated antibodies and analyzed by flow cytometry to evaluate CD62L and CD44 surface expression in total CD4 T cells (excluding aGalCer+TCR β + and CD25+ cells) in the spleen of control ($n = 4$) and *Tet2/3* DKO mice ($n = 4$). **c** Graph indicating the % of naïve (CD62L + CD44 $^-$) T cells in the spleen of control ($n = 4$) and *Tet2/3* DKO mice ($n = 3$) (p -value = 0.0011). **d** Total CD4 cells (excluding aGalCer+TCR β + and CD25+ cells) were isolated by FACS sorting from spleens of control and *Tet2/3* DKO mice. Total RNA was isolated and RNA sequencing was performed to discover differentially expressed genes. MA plot depicting differentially expressed ($p_{adj} < 0.01$) genes in *Tet2/3* DKO CD4 cells compared to control total CD4 cells isolated from spleen. WT $n = 5$, *Tet2/3* DKO CD4 cells $n = 5$. **e** 5hmC enrichment (evaluated by CMS-IP in naïve CD4 cells) in genes that are downregulated in *Tet2/3* DKO T cells (in magenta), in all the genes (in black) and in genes that are upregulated in *Tet2/3* DKO CD4 T cells (in turquoise). TSS indicates transcription start site and TES indicates transcription end site. **f** Total RNA was isolated from total CD4 (excluding aGalCer+TCR β + and CD25+ cells) cells that were purified by FACS sorting from the spleen of control or *Tet2/3* DKO mice. Real-time RT-qPCR evaluating gene expression of *Batf3* ($n = 3$ per genotype), *Irf4* ($n = 2$ per genotype, p -value = 0.0021), *Hes1* ($n = 3$ per genotype) and *Tet1* ($n = 3$ per genotype, p -value = 0.0363) in control and *Tet2/3* DKO total CD4 cells. **g** Spleens were isolated from control and *Tet2/3* DKO mice and were dissociated to create

single-cell suspensions. Cells were stained with fluorescent-labeled antibodies against cell surface proteins to identify total CD4 cells (excluding aGalCer+TCR β + and CD25+ cells). Then intracellular staining was performed with fluorescent-conjugated antibody against the transcription factor IRF4. Flow cytometry data assessing the expression of IRF4 in control and *Tet2/3* DKO total CD4 T cells is shown. **h** Graph indicating the median fluorescence intensity (MFI) of IRF4 in CD4 T cells isolated from the spleen of control ($n = 4$) and *Tet2/3* DKO mice ($n = 4$). Paired *t*-test was performed to assess statistical significance (p -value = 0.0051). **i** Flow cytometry assessing the expression of Ki67 in control and *Tet2/3* DKO total CD4 T cells prepared from spleens as in **g**. **j** Graph indicating the MFI of Ki67 in CD4 T cells in the spleen of control ($n = 4$) and *Tet2/3* DKO mice ($n = 4$) (p -value = 0.0004). **k** Flow cytometry assessing the expression of MYC in control and *Tet2/3* DKO total CD4 T cells isolated from spleens as in **g**. **l** Graph indicating the MFI of MYC in CD4 T cells in the spleen of control ($n = 4$) and *Tet2/3* DKO mice ($n = 4$). **m** Flow cytometry assessing the expression of ROR γ t in control and *Tet2/3* DKO total CD4 T cells isolated from spleens. **n** Graph indicating the MFI of ROR γ t in CD4 T cells in the spleen of control ($n = 4$) and *Tet2/3* DKO mice ($n = 4$). **o** Flow cytometry assessing the expression of GATA3 in control and *Tet2/3* DKO total CD4 T cells. **p** Graph indicating the MFI of GATA3 in CD4 T cells in the spleen of control ($n = 4$) and *Tet2/3* DKO mice ($n = 4$). Male and female mice were evaluated with similar findings. Unless otherwise indicated, young mice (average 25 days old) shortly after weaning were analyzed. Bar graphs represent the mean \pm standard error (SEM). Unless otherwise indicated, unpaired *t*-test was performed to evaluate statistical significance ($p < 0.05$ (*); < 0.01 (**); < 0.001 (***)). Unless otherwise indicated, the statistical analysis revealed no significance. For flow cytometry and qPCR experiments at least two independent experiments were performed.

mice showed splenomegaly and lymphadenopathy (Fig. 2b). Histological analysis of spleen and lymph nodes revealed that the recipients exhibited hallmarks of lymphoproliferative disorder. Specifically, they showed pleomorphic cytology, characterized by enlarged cells, with prominent nucleoli and increased euchromatin, characteristic of dedifferentiation (Fig. 2c). Harvesting and dissociation of spleen and lymph nodes further confirmed increased number of cells in the organs isolated from the recipient mice of *Tet2/3* DKO T cells compared to age and sex matched control mice who had not received *Tet2/3* DKO cells (Fig. 2d). Assessment of CD45.1 and CD45.2 expression in different recipients by flow cytometry confirmed the significant expansion of the CD45.2 $^+$ donor cells in spleen (Fig. 2e) as well as in lymph nodes (Fig. 2f).

For the second transplantation, we isolated CD45.2 $^+$ cells that have been already expanded for 16 weeks in recipients, by FACS sorting (Supplementary Fig. 4) and re-transplanted them in new CD45.1 $^+$ immunocompetent recipients (Fig. 2a). The second transplantation resulted in significant acceleration of the expansion of the transplanted cells which became apparent within 2–4 weeks (Fig. 2a). Similarly, mice that received cells that had already expanded showed increased cell numbers of spleen and lymph nodes (Fig. 2g) at an accelerated period. Evaluation of the frequency of CD45.1 $^+$ and CD45.2 $^+$ cells by flow cytometry in spleen (Fig. 2h) and lymph nodes (Fig. 2i) indicated the expansion of the donor cells.

***Tet2/3* DKO expanded cells exhibit chromosomal copy number variations**

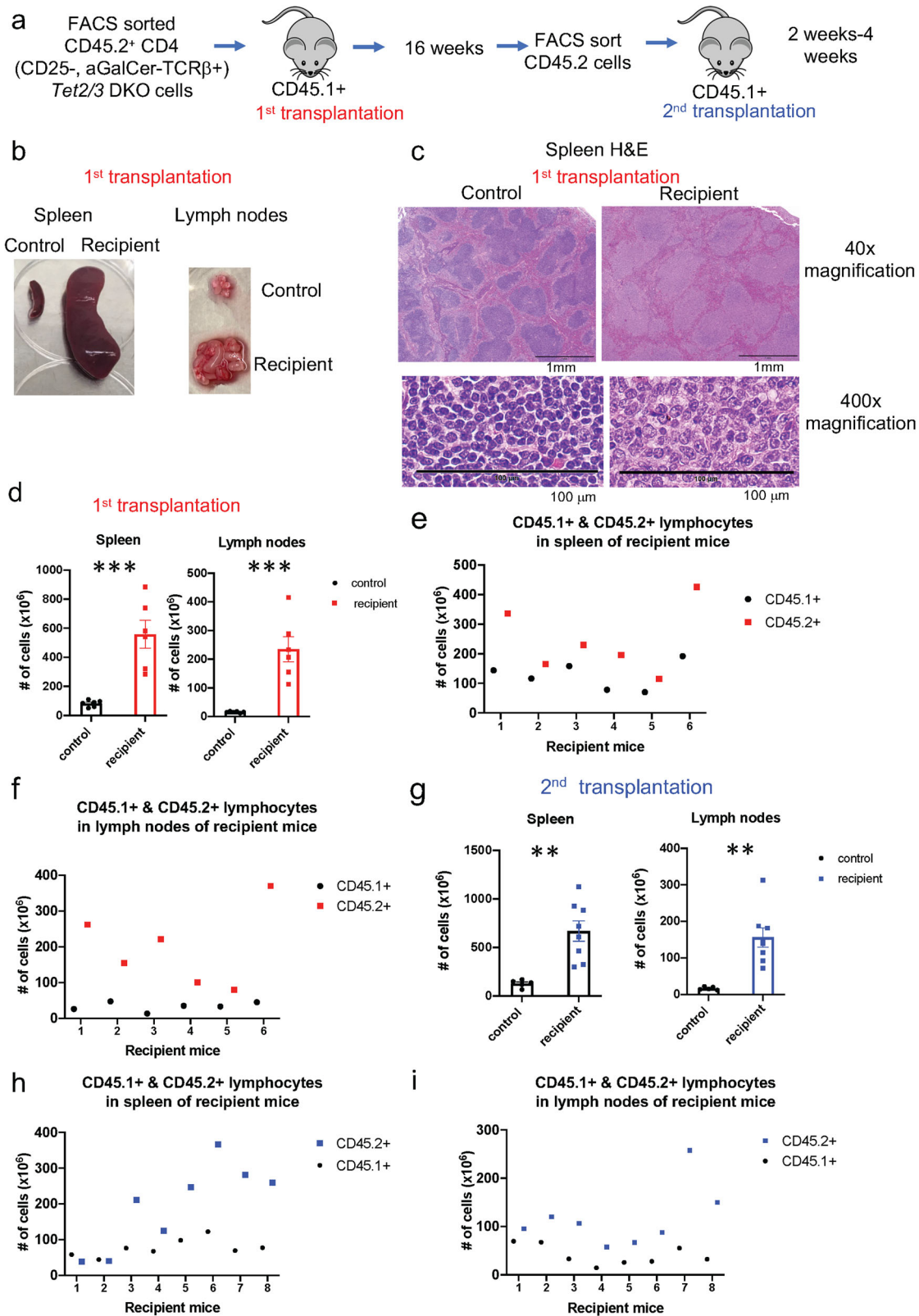
The striking pleomorphic appearance of the expanded cells in our histological analysis (Fig. 2c) indicated variable size and shape of the cells and an increased size of the nucleus. These findings prompted us to investigate if the *Tet2/3* DKO CD4 cells demonstrated chromosomal copy number variations (CCN). To this end, we performed low coverage, whole genome sequencing using three biological replicates of sorted total CD4 T cells (as defined in Supplementary Fig. 2) from wild type mice (control), three biological replicates of expanded *Tet2/3* DKO CD4 T cells (Supplementary Fig. 4) after one transplantation and four biological replicates of expanded *Tet2/3* DKO T cells after two transplantations. The analysis of the representation of somatic chromosomes using CNVkit³⁹ revealed aneuploidies in all the *Tet2/3* DKO T cells that have been transplanted and expanded in recipients. Specifically, our analysis revealed that these samples demonstrated gain of at least one copy of chromosomes (Fig. 3). While gain of chromosome 17 was

shared among all the samples that were analyzed (Fig. 3), additional CCN alterations were detected such as increase of chromosomes 2, 4, 6, 15 and 16. Our data demonstrated that expanded *Tet2/3* DKO T cells exhibited loss of genomic integrity.

***Tet2/3* DKO expanded cells upregulate genes involved in proliferation and stemness and downregulate CD4 and TCR β**

We investigated the alterations in the gene expression profile of the expanded cells upon serial transplantations. Expanded *Tet2/3* DKO cells in the first transplantation have 6641 DEGs among which 3647 are upregulated and 2994 are downregulated (Fig. 4a). We expanded this analysis to assess gene expression changes in *Tet2/3* DKO cells that have been re-transplanted to new recipients and have demonstrated accelerated disease emergence and progression. Our analysis showed that 4733 genes were upregulated and 4460 genes were downregulated compared to wild type cells (Fig. 4b). Among the upregulated genes we identified *Batf3*, *Irf4*, *Hes1*, *Mki67*, *Rorc*, *Gata3*, *Il4* as well as members of the *Lmo* family, such as *Lmo2*, *Lmo4* and *Lmo7* (Fig. 4a–c). Among the downregulated genes we identified *Tet1*, *Bcl11b*, *Cd4* and *Satb1* (Fig. 4a–c). In addition, the expanded *Tet2/3* DKO cells showed significant increase in the expression of the proto-oncogene *Myc*, that could be attributed, at least partially, to the persistent upregulation of IRF4 and BATF3³¹ (Fig. 4a, b). Gene set enrichment analysis (GSEA) for hallmark *Myc* targets revealed significant upregulation in expanded *Tet2/3* DKO cells that gradually increased upon serial transplantation (Supplementary Fig. 5a, b). We investigated the expression of these genes in control, *Tet2/3* DKO CD4 T cells isolated from young mice and expanded cells in the first and second transplantation (Fig. 4c). Our data indicated a progressive downregulation of *Bcl11b* and *Satb1* whereas *Cd4* was similarly expressed in control and young *Tet2/3* DKO CD4 T cells, however its expression was diminished specifically in expanded cells (Fig. 4c). *Hes1* and *Lmo7* already gain expression at the young *Tet2/3* DKO CD4 T cells, whereas *Lmo2* and *Lmo4* are upregulated in expanded and transplanted *Tet2/3* DKO T cells (Fig. 4c).

We confirmed by qPCR the upregulation of *Batf3*, *Irf4*, *Hes1*, *Ki67*, *Lmo2* and the downregulation of *Satb1*, *Bcl11b* and *Tet1* (Fig. 4d–k). We note that the p -value of the unpaired *t* test was not significant for *Batf3* for first and second transplantation and for *Hes1* for the first transplantation. We attribute this to the fact that the three biological replicates that were analyzed exhibited variability. However, for *Batf3* expression a minimum of



thirty-fold increase was observed in transplanted cells compared to the control. In the case of *Hes1* expression a minimum of 4.47 fold increase was observed in the transplanted cells compared to the control.

Given the fact that the expanded *Tet2/3* DKO cells exhibited loss of genomic integrity and upregulation of proto-oncogenes we proceeded to investigate if the *Tet2/3* DKO CD4 cells gain a stemness signature, which is a

characteristic of malignant cells. First, we performed GSEA analysis comparing DEG of *Tet2/3* DKO peripheral CD4 cells to a list of 922 upregulated genes in Lineage⁻ Sca1⁺cKit⁺ (LSK) cells, compared to differentiated hematopoietic cells⁴⁰ (Supplementary Data 2 and Supplementary Fig. 5c). This comparison further revealed that *Tet2/3* DKO CD4 peripheral CD4 T cells acquire a gene expression profile that has similarities with the gene

Fig. 2 | *Tet2/3* DKO T cells can proliferate upon serial transplantations in immunocompetent recipients. **a** Schema outlining the experimental steps of the serial transplantations of *Tet2/3* DKO CD4 T cells in congenic CD45.1+ recipients. CD4+, CD25-, aGalCer β tetramer- cells were isolated by FACS sorting from young *Tet2/3* DKO mice, shortly after weaning (average age 25 days old). Cells were transplanted to CD45.1+ mice (first transplantation). 16 weeks later CD45.2+ cells, representing donor *Tet2/3* DKO T cells, were isolated by FACS sorting and were transferred to CD45.1+ recipient mice (second transplantation). For the second transplantation, organs were collected and analyzed between two and four weeks post transplantation. The mouse cartoon was obtained by openclipart.org (under Creative Commons Zero 1.0 Public Domain License). **b** Representative pictures depicting enlarged spleen and lymph nodes isolated from recipients of CD45.2+ total CD4 T cells (excluding aGalCer+TCR β + and CD25+ cells) after the first transplantation. Spleen and lymph nodes isolated from control, non transplanted mice are included for reference. **c** Hematoxylin and eosin staining (H&E) of sections of spleen isolated from control and *Tet2/3* DKO CD4 congenic recipients after first transplantation. 40 \times magnification (upper panel, scale bar represents 1 mm) or 400 \times magnification (lower panel, scale bar represents 100 μ m) is shown. **d** Splens and lymph nodes were harvested from control mice and recipient mice of *Tet2/3* DKO CD4 cells. The organs were dissociated to obtain single cell suspensions and samples were counted. Graphs depicting total number of cells from dissociated spleens (right) and lymph nodes (left) isolated from control (black, $n = 6$) and recipients of *Tet2/3* DKO CD4 cells after first transplantation (red, $n = 6$). Each dot represents a mouse. Male and female mice were evaluated with similar findings. Unpaired t-test was used to assess statistical significance. P -value = 0.0006 for spleen samples and p -value = 0.0005 for lymph nodes. **e** To assess the absolute numbers of donor (*Tet2/3* DKO CD45.2+ T cells) versus host (CD45.1+) cells in the recipient mice, single cell

suspensions from spleen were depleted of erythrocytes. Then single cell suspensions obtained from spleen and lymph nodes of recipient mice after first transplantation were stained with fluorescent antibodies to distinguish donor (CD45.2+) from host (CD45.1+) cells. Graph depicting the number of CD45.1+ (black) and CD45.2+ (red) lymphocytes in spleens and lymph nodes of recipient mice ($n = 6$) 16 weeks after the first transfer of *Tet2/3* DKO total CD4+ T cells. Each dot represents cells from one mouse. **g** Splens and lymph nodes were isolated from control and recipients of expanded CD45.2+ *Tet2/3* DKO T cells. The organs were dissociated to obtain single cell suspensions and the samples were measured to acquire cell counts. Graphs indicating the total number of cells from dissociated spleens (right) and lymph nodes (left) isolated from control (black, $n = 5$) and recipients of expanded CD45.2+ cells (blue, $n = 8$) are shown. Each dot represents a mouse. Unpaired t-test was performed to evaluate statistical significance. P -value = 0.0022 for spleen and p -value = 0.0018 for lymph nodes. **h** To check the absolute numbers of donor (*Tet2/3* DKO CD45.2+ T cells) versus host (CD45.1+) cells in the recipient mice after second transplantation, single cell suspensions from spleen were depleted of erythrocytes. Then single cell suspensions obtained from spleen and lymph nodes of recipient mice after second transplantation were stained with fluorescent antibodies to distinguish donor (CD45.2+) from host (CD45.1+) cells. Graph depicting the number of CD45.1+ (black) and CD45.2+ (blue) lymphocytes in spleens and lymph nodes of recipient mice ($n = 8$). Mice 1 and 2 were sacrificed two weeks after secondary transfer of expanded CD45.2+ T cells and mice 3–8 were sacrificed 4 weeks after the secondary transfer. Male and female mice were evaluated with similar findings. Bar graphs represent the mean \pm standard error (SEM). Unpaired t-test was performed to evaluate statistical significance ($p < 0.05$ (*); < 0.01 (**); < 0.001 (***) ; < 0.0001 (****)).

expression program of early precursor stem cells. Strikingly, when we interrogated the serially transplanted and expanded *Tet2/3* DKO cells for acquisition of stemness signature, we observed an increased overlap compared to the gain of stemness signature observed in the *Tet2/3* DKO CD4 cells that were adoptively transferred (Supplementary Data 2 and Supplementary Fig. 5d, e). For instance, we identified significant upregulation of *Meis2*, *Myb*, *Myc*, *Runx2*, *Dlk1*, *Spry2*, *Mybn*, *Il17rc*, and *Cdk6* (Fig. 4l, Supplementary Data 2). *Myc* is not upregulated in young *Tet2/3* DKO T cells. The rest of these “stemness genes” start to become upregulated in young *Tet2/3* DKO T cells (Fig. 4l).

In addition, we investigated at the protein level the expression of CD4 and TCR β at the surface of expanded cells during the first (Fig. 4m, n) and the second transplantation (Fig. 4o, p). Our data indicated that CD45.2+ cells have lost CD4 expression. This could be due to methylation of enhancers that are critical for CD4 expression⁴¹ and/or could demonstrate further the de-differentiation of cells. CD45.2+ expanded cells maintained TCR β expression, but there was a statistically significant reduction of the expression of TCR β (Fig. 4m–p).

As mentioned above, among the upregulated genes in expanded *Tet2/3* DKO T cells upon first and secondary transplantation we identified genes involved in proliferation such as *Myc*, *Irf4*, *Ki67* as well as genes such as *Gata3* and *Il-4*, which are critical for Th2 function (Fig. 4a, b). We confirmed these findings at the protein level. We established an in vivo expansion system for the CD45.2+ *Tet2/3* DKO expanded cells. We performed serial transplantation of 500,000 cells in immunocompetent CD45.1 recipient mice. CD45.2+ cells were expanded and mice were evaluated between 7–14 days post transfer (Fig. 5a). Our data indicated that at the protein level that the vast majority of the expanded cells showed increased expression of MYC (Fig. 5b, c), IRF4 (Fig. 5d, e) and Ki67 (Fig. 5f, g). We also assessed the expression of lineage specifying factors GATA3 (Fig. 5h, i) and ROR γ t (Fig. 5j, k). Collectively, our results confirmed that expanded cells significantly upregulated the expression of the examined proteins.

As GATA3 in peripheral T cells is critical for acquisition of T helper (Th) 2 identity⁴² we asked if the *Tet2/3* DKO expanded T cells produced more IL-4 in vitro. To this end, we cultured splenocytes from control and recipient mice of expanded *Tet2/3* DKO T cells in the presence or absence of phorbol 12-myristate 13-acetate (PMA) and ionomycin. We assessed IL-4 production by flow cytometry in control CD4 and expanded *Tet2/3* DKO

T cells in the presence or absence of phorbol 12-myristate 13-acetate (PMA) and ionomycin. Our data confirmed our RNA-seq data, indicating increased production of IL-4 by the *Tet2/3* DKO T cells (Fig. 5l–m). Interestingly, even unstimulated *Tet2/3* DKO T cells showed a spontaneous ability to produce IL-4 (Fig. 5l–m), consistent with the increased expression of GATA-3 (Fig. 5h, i). Although IL-4 is upregulated, it remains to be tested whether this is a major driver in the hyperproliferative response and affect host immune cell activation.

Single-cell transcriptomics reveals alterations of the immune environment upon expansion of *Tet2/3* DKO T cells

Next, we asked how the immune environment of the host changed as the hyperproliferative *Tet2/3* DKO T cells expanded. To address this question in an unbiased manner, we investigated the host immune cells in the spleen by single-cell RNA-seq after transfer of expanded CD45.2+ *Tet2/3* DKO T cells at distinct time points post transfer. Specifically, *Tet2/3* DKO CD45.2+ T cells were transferred in recipients 2 days (early time point) and 10 days (late time point) before isolating splenocytes from recipient CD45.1+ mice. We excluded dead cells and sorted for CD45.1+ cells that correspond to the host immune environment (Supplementary Fig. 6), while we excluded CD45.2+ cells that correspond to *Tet2/3* DKO expanded T cells. Notably, at 2 days post transfer the CD45.2+ cells could be merely detected, while they comprised almost 50% of the splenocytes at day 10 post transfer (Supplementary Fig. 6).

Approximately 5000 cells were pooled from 3 individual mice per condition, resulting in 15,000 per time point and 30,000 in total. The precise metrics of the run are provided in Supplementary Tables 1 and 2. Comparison of the libraries generated in the 3 different inlets revealed overlap, indicating that the libraries were similar and there was no processing technical variability (Supplementary Fig. 7a). Next, we compared the biological replicates in each time point. Our comparison demonstrated that all three biological replicates of the same time point (Supplementary Fig. 7b) showed overlap, demonstrating that they shared strong similarity. Comparing the two different time points we could identify differences between day 2 versus day 10 (Supplementary Fig. 7c).

We performed clustering analysis and identified 11 clusters of immune cells in our scRNA-seq data. Cell type annotation analysis based on the Immunological Genome (ImmGen) reference⁴³ revealed that there was a

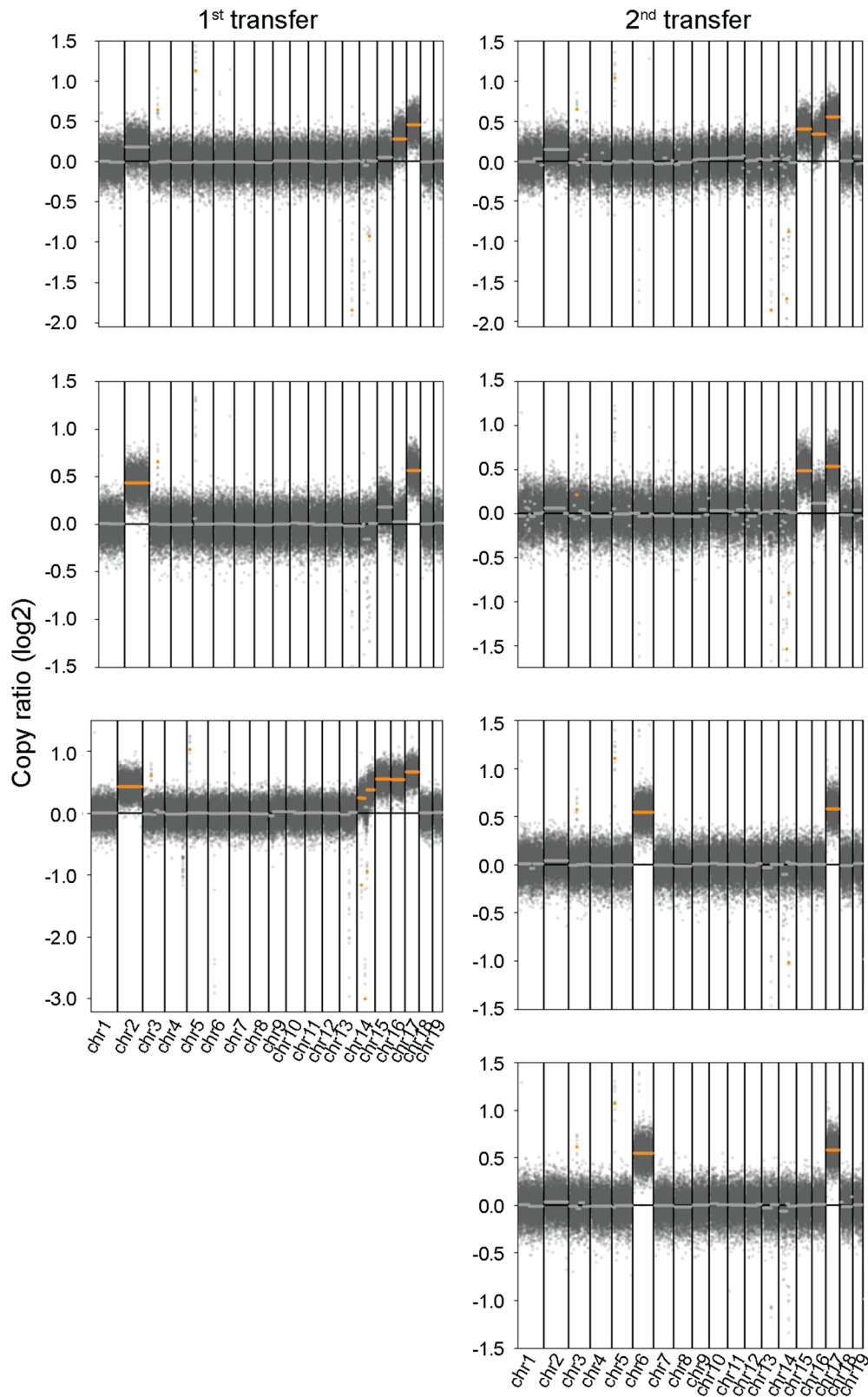
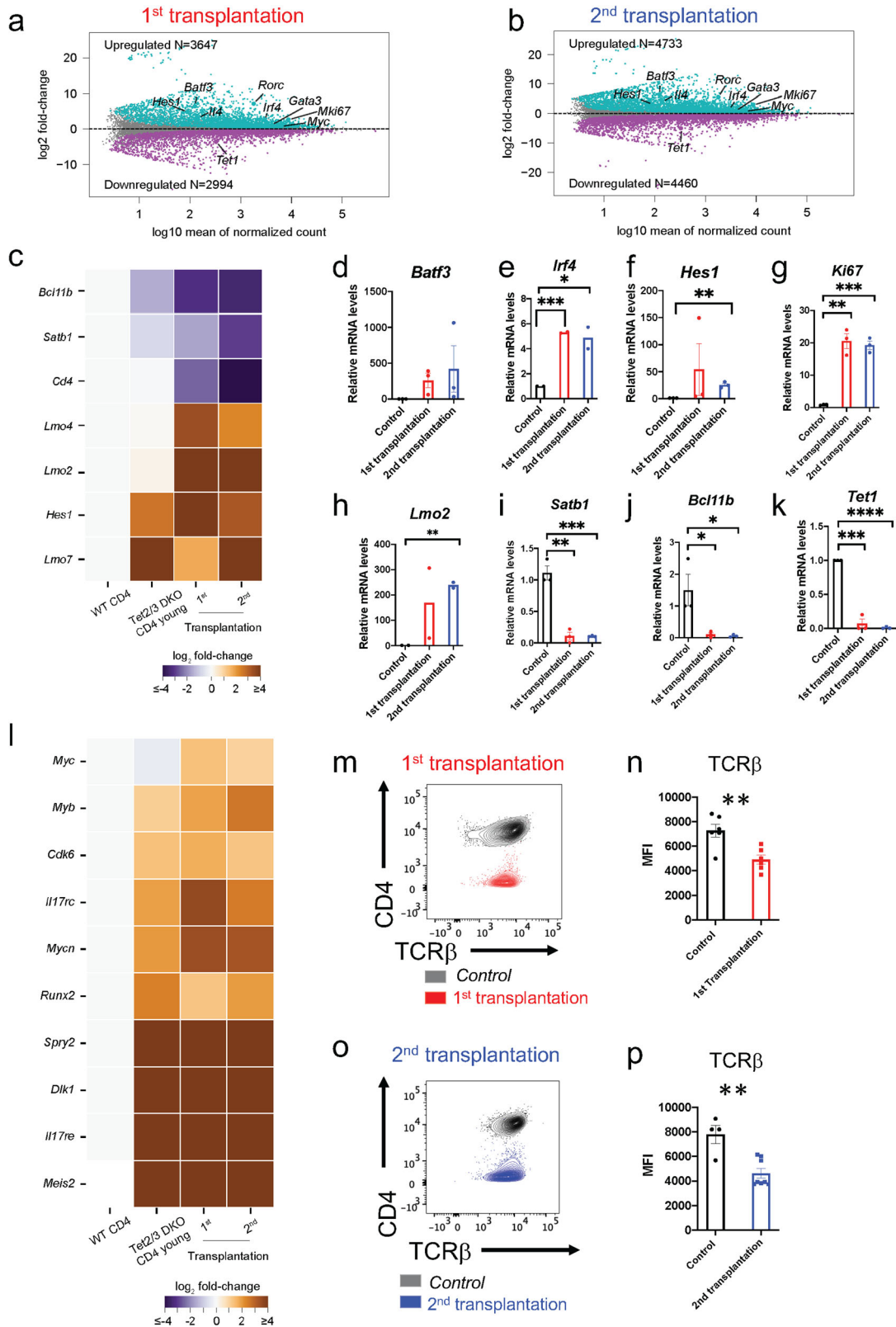


Fig. 3 | Serially transferred and expanded *Tet2/3* DKO CD4 cells exhibit chromosomal copy number alterations. Control wild type total CD4 T cells ($n = 3$), expanded donor CD45.2+ total *Tet2/3* DKO T cells after first transfer ($n = 3$) or second transfer ($n = 4$) were isolated by FACS sorting. Genomic DNA was purified

and was used without amplification for library preparation. Libraries were subjected to low coverage whole genome sequencing. Data analysis reveals aneuploidies in all the transplanted and expanded *Tet2/3* DKO T cell samples.



prominent representation of B cells, followed by T cells (Supplementary Fig. 7d, e). Other populations of adaptive immune cells were gamma delta T cells and iNKT cells. In addition, clusters of innate immunity were basophils, dendritic cells (DCs), monocytes, macrophages, neutrophils, natural killer (NK) cells and innate lymphoid cells (ILCs). When we overlaid the Uniform manifold approximation and projection (UMAP)

representation of the approximately 15,000 cells corresponding on the day 2 immune environment with the UMAP corresponding on day 10 (Fig. 6a) we were able to discern 7 major cell immune subsets, namely B cells, CD4 and CD8 T cells, NK cells, monocytes, neutrophils and DCs. When comparing the different immune populations present in the spleen of the host at day 2 versus day 10, we observed distinct clusters of the immune cell populations

Fig. 4 | *Tet2/3* DKO serially transplanted T cells upregulate genes regulating proliferation, stemness and Th2 polarization. **a** Total RNA was isolated from FACS-sorted total wild type (control) CD4 cells (excluding aGalCer+TCR β + and CD25+ cells) and CD45.2+ expanded *Tet2/3* DKO T cells (after 1st transplantation). Libraries were prepared and sequenced to identify differentially expressed genes. MA plot analysis of differentially expressed genes (DEG) in *Tet2/3* DKO expanded cells (1st transplantation) compared to control cells. Upregulated genes ($p_{\text{adj}} < 0.01$, $n = 3647$, *turquoise*) and downregulated genes ($p_{\text{adj}} < 0.01$, $n = 2994$, magenta) are indicated. Genes of interest are highlighted in each group. WT $n = 5$, expanded CD45.2+ *Tet2/3* DKO cells (1st transplantation) $n = 4$. **b** Total RNA was isolated from FACS-sorted total wild type (control) CD4 cells (excluding aGalCer+TCR β + and CD25+ cells) and CD45.2+ expanded *Tet2/3* DKO T cells (after 2nd transplantation). Libraries were prepared and sequenced to identify differentially expressed genes. MA plot analysis of DEG in *Tet2/3* DKO expanded cells (2nd transplantation). Upregulated genes ($p_{\text{adj}} < 0.01$, $n = 4733$, *turquoise*) and downregulated genes ($p_{\text{adj}} < 0.01$, $n = 4460$, *magenta*) are indicated. Genes of interest are highlighted in each group. WT $n = 5$, expanded CD45.2+ *Tet2/3* DKO cells (2nd transplantation) $n = 7$. **c** Heat map representation of differentially expressed transcription factors of interest and *Cd4* in wild type (WT) CD4, *Tet2/3* DKO CD4 cells and CD45.2+ T cells isolated during the first and second transplantation (adjusted p -value < 0.01 and absolute \log_2 fold-change > 2). The z score normalized expression is shown. **d** Total RNA was isolated from FACS-sorted total wild type (control) CD4 cells (excluding aGalCer+TCR β + and CD25+ cells) and CD45.2+ expanded *Tet2/3* DKO T cells after 1st and after 2nd transplantation in CD45.1+ recipients. RT-qPCR analysis of DEG *Batf3*. **e** *Irf4* (1st transplantation p -value = 0.0001, 2nd transplantation p = 0.0001), **f** *Hes1* (2nd transplantation p -value = 0.0012), **g** *Ki67*, (1st transplantation p -value = 0.001, 2nd transplantation p -value = 0.0465), **h** *Lmo2* (2nd transplantation p = 0.0022), **i** *Satb1* (1st transplantation p -value = 0.004, 2nd

transplantation p -value = 0.0008), **j** *Bcl11b* (1st transplantation p -value = 0.0492, 2nd transplantation p -value = 0.0443) and **k** *Tet1* (1st transplantation p -value = 0.0001, 2nd transplantation p -value < 0.0001). Each dot indicates a biological replicate. At least 2 biological replicates per genotype were assessed. **l** Heat map indicating differentially expressed stemness genes identified by RNA-seq in wild type (WT) CD4, *Tet2/3* DKO CD4 cells and CD45.2+ T cells isolated during the first and second transplantation (adjusted p -value < 0.01 and absolute \log_2 fold-change > 2). The z score normalized expression is shown. **m** Splens were harvested and dissociated to obtain single cell suspensions. Cells were stained with fluorescent-conjugated antibodies and were evaluated by flow cytometry for CD4 and TCR β expression in CD45.2+ cells that have expanded in CD45.1+ congenic recipients after first transplantation. In black are shown cells from a control, non transplanted sample and in red CD45.2+ cells. **n** Graph indicating the median fluorescence intensity (MFI) of TCR β expression in control total CD4 cells (black) and CD45.2 *Tet2/3* DKO expanded CD4 T cells (red) after first transplantation ($n = 6$). Unpaired t-test was used to assess statistical significance. P -value = 0.0045. **o** Evaluation by Flow cytometry of CD4 and TCR β expression in CD45.2+ cells that have expanded in CD45.1+ congenic recipients after second transplantation. In black are shown cells from a control, non transplanted sample and in blue CD45.2+ cells. **p** Graph indicating the MFI of TCR β in control total CD4 cells (black) and CD45.2 *Tet2/3* DKO expanded cells (blue) after second transplantation ($n = 8$). Unpaired t-test was performed to assess statistical significance. P -value = 0.0017. In all graphs each dot represents a mouse. Male and female mice were assessed. Bar graphs represent the mean \pm standard error. Unpaired t-test was performed to evaluate statistical significance ($p < 0.05$ (*); < 0.01 (**); < 0.001 (***) ; < 0.0001 (****)). If no otherwise indicated, there was no statistical significance. For Flow cytometry and RT-qPCR experiments at least two independent experiments were performed.

(Fig. 6b, c) indicating differences in their global transcriptional program. The most prominent differences we observed were in gene expression of B cells, followed by T cells, as well as monocytes (Fig. 6a–c). Moreover, our data indicated changes in the number of some of the immune populations. Specifically, innate populations and in particular monocytes appear to be increased in day 10 (Fig. 6d).

We then asked which were the biological implications of the observed changes in gene expression. GSEA for the B cells revealed that the gene expression program at day 10 post transfer showed upregulation of MYC targets, increased Interferon gamma and alpha response (Fig. 6e). It has been reported that MYC is required for primary B cell differentiation and B cell proliferation^{44–46}. In addition, it has been shown that MYC, frequently in collaboration with its partner MAX, are involved in the regulation of the B cell response after activation⁴⁷. At the molecular level, it has been proposed that MYC is involved in chromatin decompaction and can regulate nuclear architecture during B cell activation⁴⁸. IFN α and IFN β have been reported to induce B-cell activation⁴⁹. Similarly, for CD8 and CD4 T cells we discovered upregulation of genes involved in IL-2/ STAT5 signaling, IFN α and IFN γ response as well as TNF α signaling via NF- κ B, indicating that processes involved in cellular activation are taking place at day 10 (Fig. 6f, g). When examining gene signatures for monocytes the predominant upregulated category at day 10 is TNF α signaling via NF- κ B (Fig. 6h). Similarly, evaluation of the gene signatures of other innate immune cell subsets, such as dendritic cells (Supplementary Fig. 7g), neutrophils (Supplementary Fig. 7h) and NK cells (Supplementary Fig. 7i) confirmed upregulation of proliferation or/ and activation at day 10 post transplantation. interestingly, for the dendritic cells we also noticed upregulation of genes involved in DNA repair and apoptosis, potentially indicating that the cells undergo stress at day 10, as the *Tet2/3* DKO T cells largely expand and take over (Supplementary Fig. 7g).

T cells in recipient mice are activated and secrete increased levels of IFN γ

Next, we focused our analysis on the T cell compartment of the recipient mice. We performed our analysis at 10 days after transplantation of serially expanded cells. At this stage we could still detect CD45.1+ cells that represent cells of the host mice (Supplementary Fig. 6). Our data indicated

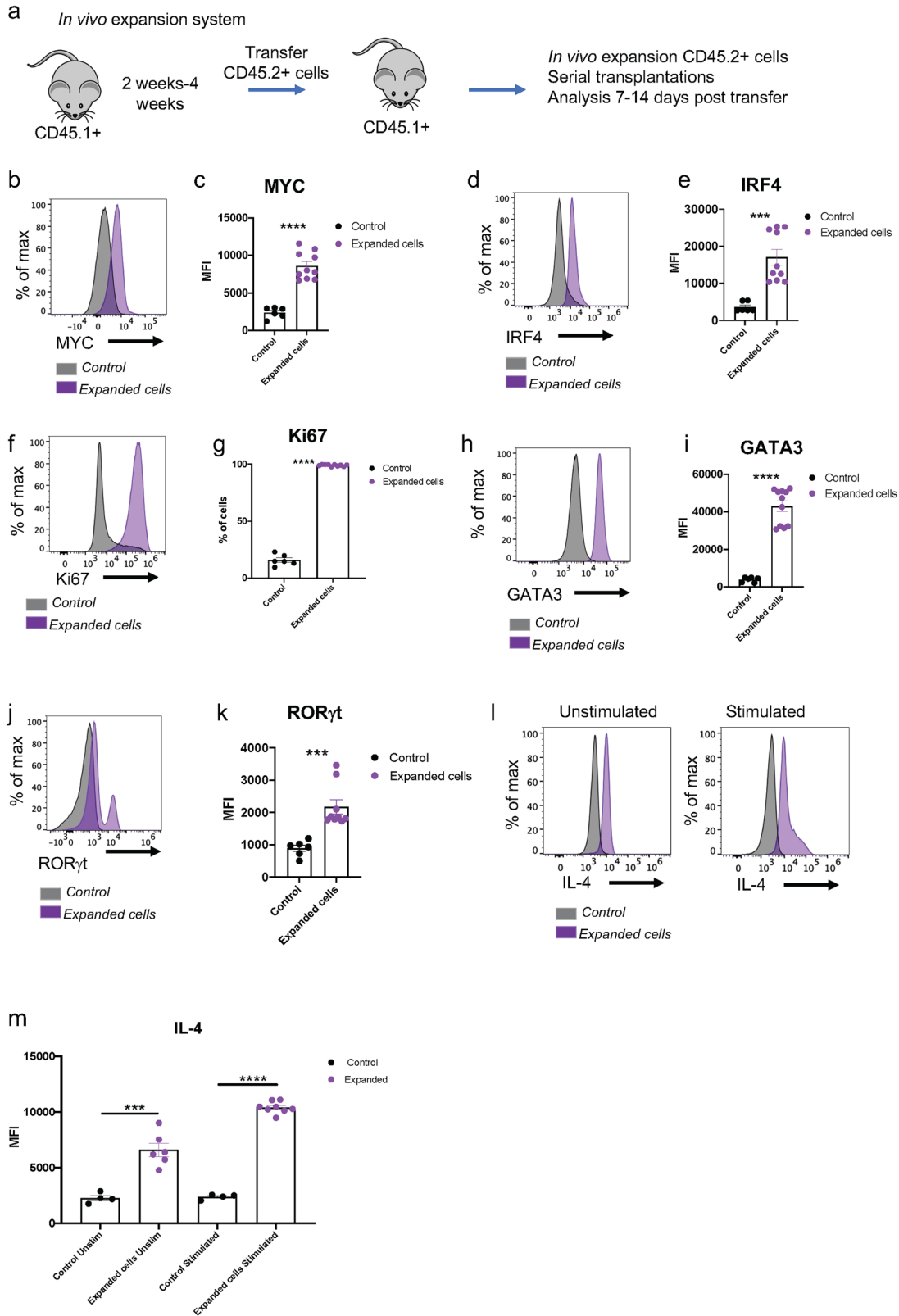
that in the recipient mice the frequency of CD4 and CD8 cells and the absolute numbers of CD4 cells were significantly reduced compared to control mice (Fig. 7a–c). Analysis based on CD44 and CD62L expression indicated that the frequency and absolute numbers of activated, CD44+CD8 cells as well as the frequency of effector/ memory CD8 cells that co-express CD44 and CD62L was increased in mice that received serially expanded *Tet2/3* DKO T cells (Fig. 7d–f). Next, we analyzed the CD4 activation status. First, we checked representation of Tregs as determined by CD4 and CD25 expression (Fig. 7g). The expression of FOXP3 was comparable between the control and the CD4+CD25+ cells in the recipient mice (Fig. 7h). The frequency of Tregs was increased in the recipient mice (Fig. 7i), potentially reflecting a response of the immune system of the host to suppress the expanding activated *Tet2/3* DKO T cells. However, the absolute numbers of Tregs were comparable (Fig. 7i). Finally, we confirmed that the frequency of CD44+ and CD44+CD62L+ activated CD4 cells was increased in the recipient mice but the total numbers were comparable (Fig. 7j–l).

In addition, we isolated splenocytes from control mice and recipient mice of serially expanded *Tet2/3* DKO T cells and stimulated the cells in vitro in the presence of PMA and ionomycin for four hours. We assessed production of IFN γ in in vitro activated, total CD8 cells by flow cytometry. Our data indicated that CD45.1+, total CD8 cells from the recipient mice produced increased numbers of IFN γ compared to total, CD8+ cells that were isolated from control mice after in vitro activation with PMA and ionomycin (Fig. 7m, n).

Thus, our phenotyping data complemented the single cell RNA-seq data to indicate activation of CD45.1+ T cells in the recipient mice. Albeit, this activation did not suffice to control the expansion of *Tet2/3* DKO T cells.

Discussion

In the present study, we investigated the impact of concomitant deletion of TET2 and TET3 in T cell proliferation and immune evasion. We also sought to discern what was the biological significance of the identified alterations in the transcriptional program of the CD4 lineage that were mediated by TET2 and TET3 loss. The challenge was to overcome the multiple immunological issues related to TET loss in T cells; such as aberrant iNKT cell development and expansion¹⁸, emergence of CD8



innate like T cells¹⁸ and the well-established instability of the regulatory T cell lineage²² that collectively resulted in an aggressive disease that caused accelerated death of the *Tet2*^{-/-}*Tet3*^{flx/flx} CD4Cre and *Tet2*^{flx/flx} *Tet3*^{flx/flx} CD4Cre mice between 7 and 8 weeks old^{18,22}. To circumvent this, we performed serial transplantations in fully immunocompetent recipients, discovering that *Tet2*^{-/-}*Tet3*KO cells exhibited hyperproliferation *in vivo*.

Overall, in our study we report defective control of T cell expansion, upon concomitant deletion of TET2 and TET3, characterized by gradual upregulation of the protooncogene Myc and gain of increased stemness signature. As a result, the CD4 cells that emerge are abnormal and susceptible to hyperproliferation. We also report that the *Tet2/3* deficient T cells exhibit aneuploidies.

Fig. 5 | Serially transplanted *Tet2/3* DKO T cells express high levels of transcription factors MYC, IRF4, GATA3 and produce IL-4. **a** Schema outlining the experimental procedure of serial transplantation. The mouse cartoon was obtained from openclipart.org (under Creative Commons Zero 1.0 Public Domain License). **b** Spleens were isolated from control or recipient mice and were dissociated to obtain single-cell suspensions. Surface staining with fluorescent-conjugated antibodies was performed, followed by intracellular staining to identify transcription factors and proliferating markers of interest. The cells were analyzed by flow cytometry. Representative histograms of MYC, **d** IRF4, **f** Ki67, **h** GATA3, **j** ROR γ t expression evaluated by flow cytometry in control CD4 T cells (gray) and expanded *Tet2/3* DKO T cells (purple) upon serial transplantations in congenic mice are shown. **c** Graph depicting median fluorescence intensity (MFI) of MYC (p -value < 0.0001), **e** of IRF4 (p -value = 0.0003), **g** Ki67 (p -value < 0.0001), **i** GATA3 (p -value < 0.0001), **k** ROR γ t (p -value = 0.0006) as determined by Flow cytometry in control CD4 T cells (gray) and expanded *Tet2/3* DKO T cells (purple) upon serial transplantations in congenic

mice. **l** Spleens were isolated from control or recipient mice and were dissociated to obtain single-cell suspensions. Cells were cultured in the presence of brefeldin A (unstimulated) or in the presence of PMA, ionomycin and brefeldin A (stimulated) for four hours. Surface staining with viability dye and fluorescent-conjugated antibodies was performed, followed by intracellular staining to identify IL-4. Representative data obtained by flow cytometry assessing IL-4 production from control CD4 T cells (gray) and expanded *Tet2/3* DKO T cells (purple) upon serial transplantations in congenic mice are shown. **m** Graphs depicting MFI of IL-4 in control CD4 T cells (gray) and expanded *Tet2/3* DKO T cells (purple) upon serial transplantations in congenic mice that were left unstimulated (p -value = 0.0005) or were stimulated (p -value < 0.0001) as determined in **l**. In all graphs each dot represents a mouse. Male mice were assessed. Bar graphs represent the mean \pm standard error. Unpaired t-test was performed to evaluate statistical significance. (p < 0.001 (**); < 0.0001 (****)). If no otherwise indicated, there was no statistical significance. At least two independent experiments were performed.

Previous studies have extensively studied the impact of TET2 deficiency in HSC proliferation and myeloid skewing^{8,11,13}. In addition, deletion of TET1 results in B cell lymphomas that appear late in the life of mice²⁷. Concomitant deletion of more than one member of the TET family of proteins can result in accelerated and aggressive phenotypes^{28,50}, suggesting redundant function of these proteins. Reduction of 5hmC can have prognostic value in blood cancers such as myelodysplastic syndromes³ and indicates the importance of the catalytic activity of TET proteins. However, recent studies reported catalytic independent roles of TET2 in the context of lymphoid malignancies and in particular B cell malignancies¹³. On the other hand, catalytic activity of TET2 was reported to be indispensable in the context of myeloid expansion^{13,14} as well as conventional and unconventional T cell lineage specification¹⁹. While the precise TET mediated tumor suppressive mechanisms are not fully elucidated, there are shared phenotypic features that characterize the TET deficient expanded cells, including the *Tet2/3* DKO T cells in this study. In summary, TET deficient cells exhibit upregulation of genes that are typically expressed in precursor stages demonstrating maintenance of stemness and they typically exhibit impaired DNA repair and characteristics of genomic instability^{18,27,28,50}.

Specifically, in this study our data indicated that TET proteins might exert direct roles in regulating genomic stability. It has been previously shown that TET deficient embryonic stem cells (ESCs) exhibited aneuploidies⁵¹. Mechanistically, this was attributed to increased methylation of the gene *Khd3*, which resulted in reduced expression of the protein that it encodes, KHDC3⁵¹. KHDC3 was reported to be involved in spindle assembly specifically in ESCs but it is not expressed in hematopoietic cells⁵¹. Future, detailed studies will shed light in the potential roles of TET proteins to regulate genomic stability in T cells. There are multiple plausible scenarios. For instance, as it has been reported in ESCs⁵¹, TET proteins might regulate the expression of genes involved in spindle assembly to ensure proper chromosome segregation. In addition, accumulation of 5hmC has been reported at sites of DNA damage⁵². It has been shown that loss of TET proteins and subsequent loss of 5hmC impairs chromosome segregation in conditions of replication stress⁵². Another possibility may be that TET proteins by generating 5hmC and other oxi-mCs promote the recruitment of proteins involved in the process of DNA repair to facilitate resolution of breaks and safeguard genomic integrity. Indeed, studies in the literature suggest that 5fC and 5caC can be preferentially bound by proteins involved in DNA repair^{53,54}. In support of these findings, we have been previously identified accumulation of double strand breaks (DSBs) and increase of R loops in *Tet2/3* DKO iNKT cells⁵⁵, whereas accumulation of DSBs has also been reported in *Tet1* deficient B cells²⁷ and HSCs that lack concomitantly all three TET proteins²⁸.

We isolated *Tet2/3* DKO CD4 T cells from young mice immediately post weaning. The spleens from control and *Tet2/3* DKO mice appeared to be of comparable size. However, we must indicate that while the majority of the *Tet2/3* DKO T cells were naïve we still observed a significant and reproducible increase of activated T cells. Genes that were upregulated in

young *Tet2/3* DKO CD4 T cells such as *Irf4* and *Batf3* are critical for upregulating MYC and this path has been linked to the emergence of T cell lymphoma³¹. Our RNA-seq data at different stages of T cell expansion demonstrated a persistent upregulation of *Irf4* and *Batf3* that lead gradually to upregulation of *Myc* in the rapidly proliferating expanded *Tet2/3* DKO T cells. Our flow cytometry data further confirmed at the protein level, that early on in *Tet2/3* DKO T cells isolated from young mice IRF4 is predominantly upregulated in a significant amount of cells and gradually IRF4 is upregulated in all the *Tet2/3* DKO T cells that expanded in serial transplantations. These cells also expressed MYC as well as Ki67 and GATA3. Intriguingly, some studies revealed the importance of activation of TET deficient cells as a contributing factor in the path to malignant transformation in mice. Specifically, in T cells activation with ovalbumin was critical for the expansion of TET2 deficient, RHO G17V T cells that expressed an OT-II TCR¹⁵. In addition, it was demonstrated that myeloid expansion in mice with a *Tet2* missense mutation that compromised catalytic activity, could be significantly accelerated by inducing inflammation through in vivo LPS administration¹⁴. Collectively the data suggested that inflammation and cell activation could act synergistically with TET loss of function to promote aberrant proliferation and malignant transformation in blood cells. Expanding on these findings, as TET2 deficient human T cells expressing chimeric antigen receptors⁵⁶ and murine TET2 KO CD8 cells⁵⁷ show enhanced memory potential and thus are considered to hold promise in the context of cancer immunotherapy, it is critical to assess the long-term impact of their activation status in their proliferative capacity.

Another feature of the serially expanded *Tet2/3* DKO T cells is the upregulation of GATA3 and the increased expression of IL-4, which are hallmarks of Th2 lineage and function^{42,58}. Interestingly, our datasets did not reveal upregulation of BCL6, a key transcription factor of the Tfh lineage^{59,60}. At a first glance, this may seem contradictory to the human data that indicate high frequency of *Tet2* mutations in AITL, a lymphoma that has characteristics reminiscent of Tfh cells⁹. However, in this type of blood cancer, *Tet2* mutations co-occur with a loss of function mutation for RHO GTPase, known as RhoG17V⁹. Studies in mice have uncovered that TET2 mutations are important for proliferation, but it is the RhoG17V form of the GTPase that drives the acquisition of the Tfh phenotype¹⁵. Interestingly, upregulation of GATA3 has been reported in a subset of PTCL-NOS, known as PTCL-GATA3⁶¹. PTCL-GATA3 is characterized by upregulation of genes involved in cell cycle and proliferation, including MYC and from loss of genomic integrity as demonstrated by aneuploidies^{61,62}.

A paradoxical finding from our RNA-seq data was the upregulation of a plethora of genes upon TET deletion. However, multiple studies have reported similar findings in other immune cells that lack TET proteins^{18,28,35,50}. There are multiple reasons that contribute to upregulation of genes and not only downregulation⁶³. Deletion of TET proteins resulted in downregulation of key transcription factors followed by upregulation of other factors that would be normally silenced. These newly upregulated transcription factors turned on their own gene expression program and

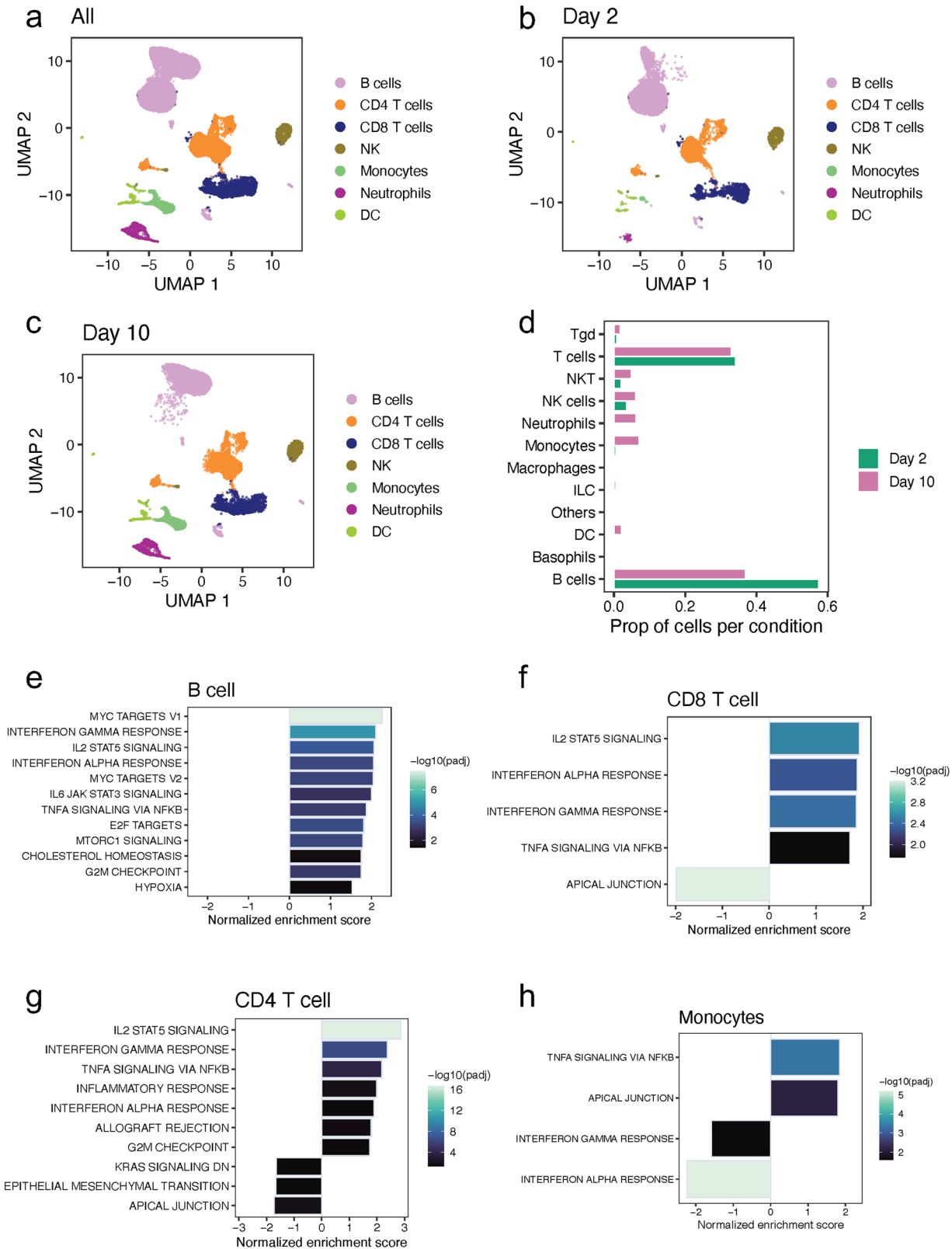
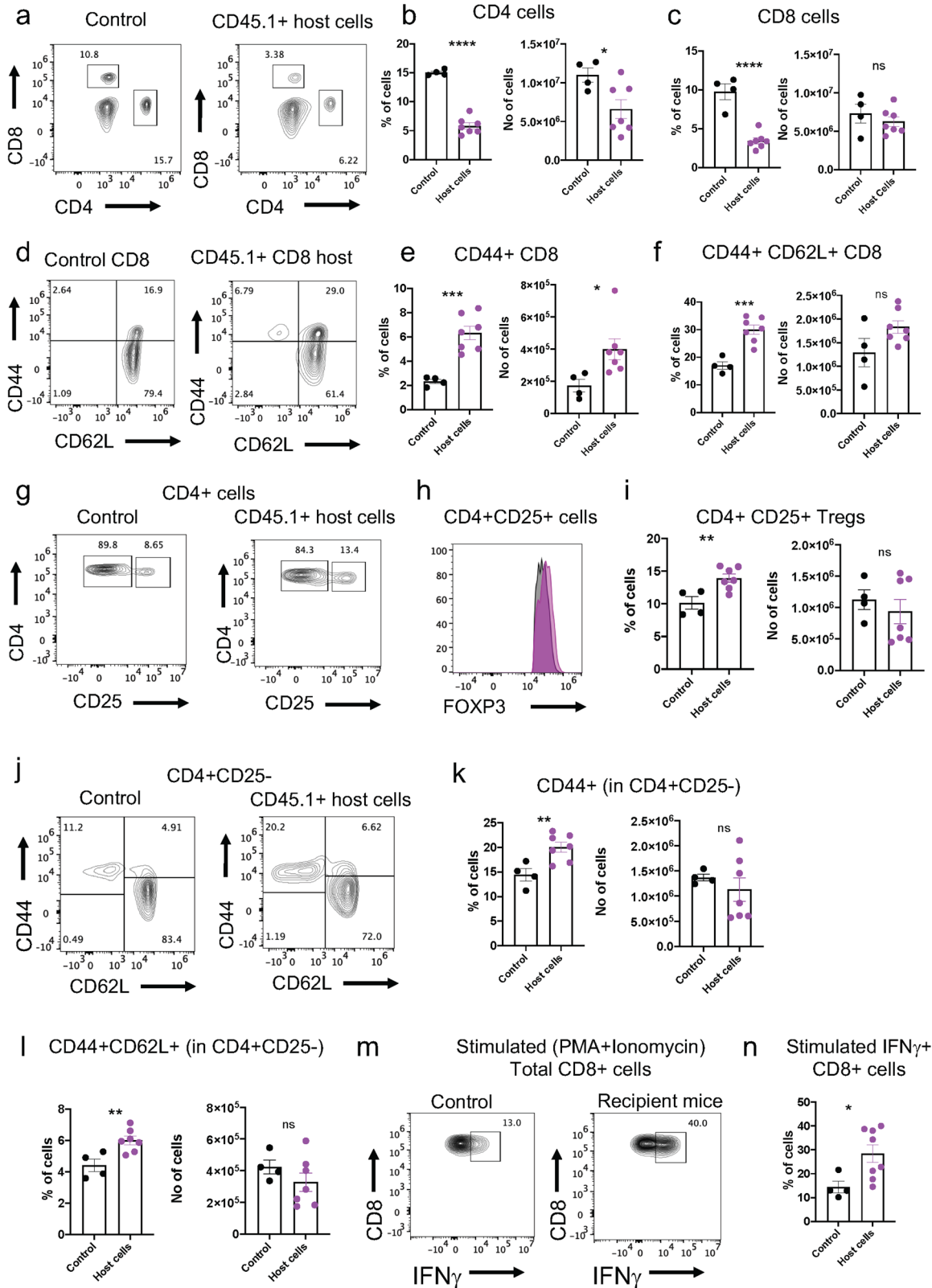


Fig. 6 | Single-cell transcriptomic analysis reveals progressive alterations of the immune landscape as *Tet2/3* DKO T cells expand in recipient mice. **a** UMAP plot of all cells. Each cluster is annotated by comparing the cluster label and the ImmGen annotation reference. **b** UMAP plot of cells from day 2 after transfer. Each cluster is annotated by comparing the cluster label and the ImmGen annotation reference. **c** UMAP plot of cells from day 10 after transfer. Each cluster is annotated by comparing the cluster label and the ImmGen annotation reference. **d** Bar plot of cell proportion per condition for each cell type. **e** GSEA results for significant Hallmark

genesets in B cells between conditions. Positive normalized enrichment score indicates more enriched in day 10 after transfer. **f** GSEA results for significant Hallmark gene sets in CD4 T cells between conditions. Positive normalized enrichment score indicates more enriched in Day 10 after transfer. **g** GSEA results for significant Hallmark genesets in CD8 T cells between conditions. Positive normalized enrichment score indicates more enriched in Day 10 after transfer. **h** GSEA results for significant Hallmark gene sets in Monocytes between conditions. Positive normalized enrichment score indicates more enriched in day 10 after transfer.



upregulate the genes that they control^{6,18,37}. Moreover, we identified downregulation of critical factors involved in chromatin organization and gene expression such as SATB1 and BCL11B, that exert complex roles in regulating gene expression⁶⁴⁻⁷⁰. TET deficient cells typically exhibited altered fate choices compared to their wild type/ control counterparts, frequently maintained expression of genes characterizing precursor states^{18,63}. This also

resulted in upregulation of genes. TET deficient cells were typically prone to DNA repair defects and they upregulated genes involved in DNA repair^{18,27,28,52,55,71}.

We asked how the differentially expressed genes would correlate with loss of 5hmC. We have previously demonstrated that *Tet2/3* DKO T cells in these mice showed reduction of 5hmC¹⁸. In addition, in the present study we

Fig. 7 | T cells of the recipient mice become activated as serially transplanted *Tet2/3* DKO T cells expand. **a** Spleens were harvested from control and CD45.1+ recipients of serially transplanted *Tet2/3* DKO T cells. Single cell suspensions were prepared by mechanical dissociation and stained with fluorescently-labeled antibodies was performed. Representative flow cytometry analysis evaluating CD4 and CD8 expression in spleen of control and in the CD45.1+ host cells in spleens isolated from recipients of serially transplanted *Tet2/3* DKO T cells is shown. **b** Graphs depicting frequency (p -value < 0.0001) and absolute numbers (p -value = 0.0352) of CD4 cells as defined in **a**. **c** Graphs depicting frequency (p -value < 0.0001) and absolute numbers of CD8 cells as defined in **a**. **d** Flow cytometry analysis assessing CD44 and CD62L expression in CD8 cells in spleen of control and in the CD45.1+ host cells in spleens isolated from recipients of serially transplanted *Tet2/3* DKO T cells. **e** Graphs depicting frequency (p -value = 0.0006) and absolute numbers (p -value = 0.0357) of activated CD44 + CD8 cells as identified in **d**. **f** Graphs depicting frequency (p -value = 0.0006) and absolute numbers of CD44 + CD62L + CD8 cells as identified in **d**. **g** Flow cytometry analysis of CD4 + CD25 + T cells and in the CD45.1+ host cells in spleens isolated from recipients of serially transplanted *Tet2/3* DKO T cells. **h** Overlay of Foxp3 expression in CD4 + CD25 + T cells as identified in **g**. **i** Graphs

representing the frequency (p -value = 0.0079) and absolute numbers of CD4 + CD25 + T cells as identified in **g**. **j** CD44 and CD62L expression in CD4 + CD25- cells in spleen of control and in the CD45.1+ host cells in spleens isolated from recipients of serially transplanted *Tet2/3* DKO T cells. **k** Frequency (p -value = 0.0082) and absolute numbers of activated CD44 + CD4 cells as identified in **j**. **l** Frequency (p -value = 0.0081) and absolute numbers of activated CD44 + CD62L + CD4 cells as identified in **j**. **m** Spleens were isolated from control mice and recipient mice of serially transplanted *Tet2/3* DKO T cells. Cells were isolated and stimulated in vitro with PMA and ionomycin in the presence of brefeldin A for four hours. After cell surface staining, intracellular staining was performed by Flow cytometry in total CD8+ cells to assess IFN γ expression in control and recipient mice. **n** Graph representing the frequency of PMA and ionomycin activated total CD8 + IFN γ + cells as identified in **m**. (p -value = 0.0347). Male mice were evaluated. In all graphs each dot represents a mouse. Bar graphs represent the mean \pm standard error. Two independent experiments were performed with $n = 4$ (black) for control and $n = 8$ (magenta) for host cells of recipient mice. Unpaired t-test was performed to evaluate statistical significance ($p < 0.05$ (*); < 0.01 (**); < 0.001 (***) ; < 0.0001 (****), ns no significance).

demonstrated that *Tet1* is downregulated resulting in gradual loss of expression of all three TET proteins. Our data revealed a correlation of 5hmC distribution in wild type cells with reduced gene expression in *Tet2/3* DKO CD4 T cells. However, in this study we did not attempt to make additional links with DNA modification status since we believe that the present system of expanded cells we used hindered the identification of causal links between the loss of TET proteins and changes in DNA methylation. Specifically, we previously performed WGBS in *Tet2/3* DKO iNKT cells¹⁸. Our initial analysis indicated similar CpG methylation levels consistent with reports that in primary cells there is prevalent hypermethylation at the CpG level⁷². However, only when we focused on developmentally different regions between HSCs and thymic iNKT cells we were able to identify some meaningful changes in DNA methylation, indicating that the action of TET proteins is specific¹⁸. These changes were meaningful in the context of iNKT cell lineage specification, however they did not shed light on the gain of proliferation of these cells¹⁸. Indeed, a specific catalytic activity of TET proteins to promote DNA demethylation of selected enhancers is broadly accepted⁷³. It has been previously shown in *Tet2/3* DKO iNKT cells¹⁸, *Tet2/3* DKO Tregs³⁵, *Tet2/3* DKO HSCs²⁸, *Tet1/2* deficient expanded B cells⁵⁰ there is no correlation with changes in DNA modification and gene expression⁷⁴. This paradox reveals the complex impact of TET proteins on regulating gene expression and ultimately cell fate and function. The observed phenotypes do not merely reflect the impact of TET deletion on regulating DNA modification. Instead, these phenotypes result from the combined effect of TET-mediated changes in gene expression as well as changes in gene expression due to altered transcriptional networks. Moreover, TET deficient cells typically gain proliferative traits^{6,11,12,18,26,27,50}. We and others have previously demonstrated that 5hmC is passively diluted during proliferation^{16,75}.

As the TET deficient T cells become hyperproliferative they can expand rapidly in the immune-competent host, within a few weeks. This increased proliferation sparked our interest to interrogate the role of the host's immune environment. We investigated how the gene expression of the immune cells of the host changed as TET deficient cells expanded by utilizing single cell transcriptomics at distinct time points post transfer. Our results indicated that cells of both innate and adaptive immunity exhibited significant gene expression changes that set the stage for their activation and the secretion of cytokines aiming to control the expansion of the *Tet2/3* DKO T cells. Further characterization of the host immune cells by flow cytometry revealed the acquisition of effector characteristics by both CD4 and CD8 T cells of the host, accompanied by increased secretion of IFN γ . In spite of these changes in the immune response of the host, the *Tet2/3* DKO T cells were not controlled and they expanded.

Collectively, in this report we demonstrate that *Tet2/3* DKO T cells can expand upon serial transplantation to recipient mice and they progressively gain hyperproliferative traits, accompanied by upregulation of Myc

signature gene expression program and loss of genomic integrity. Our data establish TET2 and TET3 as critical tumor suppressor genes in T cells in vivo.

Methods

Mice

The mice used in this study were bred and maintained under specific pathogen-free conditions at University of North Carolina (UNC) Genetic Medicine building, in a facility managed by the Division of Comparative Medicine at UNC Chapel Hill. The experimental procedures using mice were conducted in accordance with our approved protocol 22-252 by the UNC Institutional Animal Care and Use Committee. We have complied with all relevant ethical regulations for animal use. C57BL/6 (B6) (stock number: 000664, RRID: IMSR_JAX:000664) were initially purchased from Jackson Laboratories and were bred and maintained in our facility. B6.SJL-CD45.1 (stock number: 002014, RRID: IMSR_JAX:002014) were purchased from Jackson labs and were either bred and used from our colonies or ordered from Jackson labs and used for our experiments. *Tet2*^{-/-} mice¹¹ were initially generated by the Rao lab and were purchased from Jackson laboratory (stock number: 023359, RRID: IMSR_JAX:023359). *Tet3*^{flx/flx} mice were generated in the Rao lab (and are currently available from Jackson laboratory, stock number: 031015, RRID: IMSR_JAX:031015). We have described the generation of *Tet2*^{-/-} *Tet3*^{flx/flx} CD4Cre¹⁸ mice in previous publications. For all the experiments, *Tet2*^{-/-} *Tet3*^{flx/flx} CD4Cre were used immediately after weaning, between 22-27 days old. For genome-wide sequencing experiments, we used sex and age-matched mice. When feasible, both male and female mice were used as indicated in the specific methods sections. Specifically, for flow cytometry analysis, histology and bulk RNA-seq experiments both male and female mice were evaluated. For single cell RNA sequencing male mice were analyzed. For adoptive transfer experiments, mice were closely monitored and euthanized when they reached specific endpoints, such as reduced motility, problems in breathing, increased temperature. For our experiments, the genotype of the mutant mice was confirmed by PCR genotyping. Briefly, murine tissue was isolated and genomic DNA was extracted using Phire Animal Tissue Direct PCR kit (Thermo scientific, cat no F-140WH), following the protocol provided by the manufacturer. PCR amplification of DNA fragments was performed using the Phire DNA polymerase (Thermo scientific) and specific primers using Biorad T100 or Biorad C1000 Touch thermocyclers. PCR products were run in a 3% agarose gel and were visualized using SYBR safe (Invitrogen, Thermo Scientific) staining using an Axygen Gel documentation system.

Flow cytometry

Staining of splenocytes and cells isolated from lymph nodes was performed directly ex vivo. Briefly, mice were euthanized and organs (spleen, lymph nodes) were harvested. Single-cell suspensions were prepared by

dissociating the organs using a 70µm cell strainer (Falcon) as previously described⁷⁸. For the spleen suspension, erythrocytes were depleted using ACK lysing buffer (Life Technologies). For staining samples isolated from spleen or lymph nodes, cells were incubated for 10 min with TruStain Fc PLUS (anti-mouse CD16/32, clone: S17011E, Biolegend, RRID: AB_2783138) at room temperature. For surface stainings, cells were stained in FACS buffer (PBS containing 2% FBS). Dead cells were excluded by using fixable viability dye (fixable viability dye eFluor780, cat. no: 65-0865-18, eBioscience). To perform multiparameter Flow cytometry, antibodies were used conjugated with fluorophores: Anti-mouse CD4 Alexa Fluor (AF) 488 (clone: RM4-5, RRID: AB_389303), anti-mouse CD4 Brilliant Violet BV711 (clone: RM4-5, RRID: AB_11219396), anti-mouse CD8 BV650 (clone: 53-6.7, catalogue number: RRID: AB_11124344 and RRID: AB_465935), anti-mouse TCR-β PERCP/Cy5.5 (clone: H57-597, RRID: AB_1575173), anti-mouse B220 PE/Cy7 (clone: RA3-6B2, catalogue number: 103222, RRID: AB_313005), anti-mouse CD44 PERCP/Cy5.5 (clone: IM7, catalogue number: 103032, RRID: AB_2076204), anti-mouse CD62L BV421 (clone: MEL-14, catalogue number: 104435, RRID: AB_10900082), anti-mouse CD25 PE/Cy7 (clone: PC61, catalogue number: 102016, RRID: AB_312865), anti-CD25 APC (clone: PC61, catalogue number: 102012, RRID: AB_312861), CD45.1 PE (clone: A20, catalogue number: 110708, RRID: AB_313497), CD45.2 PE (clone: 104, catalogue number: 109808, RRID: AB_313445) or CD45.2 BV421 (clone: 104, catalogue number: 109832, RRID: AB_2565511) were all from Biolegend. The antibodies were used in a dilution 1:200 with the exception of B220 PE/Cy7 that was used in a dilution 1:300. aGalactosyl-ceramide loaded tetramer PE was obtained from NIH tetramer Core in a dilution 1:400.

For intracellular staining for nuclear proteins, such as transcription factors and proteins expressed in cycling cells, cells after surface staining, were fixed and subsequently permeabilized using the Foxp3/ transcription factor staining buffer set (Invitrogen, catalogue number: 00-5523-00) following the guidelines provided by the manufacturer. The following antibodies were diluted in 1X Permeabilization buffer: anti-c-Myc AF647 (Biolegend, clone: 9E10, catalogue number: 626810, RRID: AB_2888732, dilution 1:100), anti-IRF4 PE (Biolegend, clone: IRF4. 3E4, catalogue number: 646404, RRID: AB_2563005, dilution 1:100), mouse anti-Ki-67 AF488 (BD Pharmingen, clone: B56, catalogue number: 561165, RRID: AB_10611866, dilution 1:100), anti-Foxp3 PE (Invitrogen, clone: FJK-165, catalogue number: 12-5773-80, RRID: AB_465935, dilution 1:100), anti-RORγt BV421 (BD Horizon, clone: Q31-378, catalogue number: 562894, RRID: AB_2687545, dilution 1:100), anti-GATA3 PE (BD Pharmingen, clone: 560074, catalogue number: 560074, RRID: AB_1645330, dilution 1:5).

To evaluate cytokine production by Flow cytometry, splenocytes were stimulated with cell activation cocktail with Brefeldin A (Biolegend, catalogue number: 423304, 500x stock), which is a 500x pre-mixed cocktail of phorbol 12-myristate-13-acetate (PMA), ionomycin and Brefeldin A or were left unstimulated in the presence of Brefeldin A (Biolegend, catalogue number 420601, 1000x stock) for 4 h in 10% FBS T cell medium as previously described⁷⁸. Then, following surface staining to detect specific proteins of interest, cells were fixed and permeabilized using the Intracellular Fixation and Permeabilization buffer set (Invitrogen, catalogue number: 88-8824-00) as previously described⁷⁸. We used the following antibodies to detect proteins in the cytoplasm of the cells: anti-IL-4 AF488 (Biolegend, clone: 11B11, catalogue number: 504109, RRID: AB_493320, dilution 1:100), anti-IFNγ (Biolegend, clone: XMG1.2, catalogue number: 505832, RRID: AB_2734492, dilution 1:100).

Samples were analyzed by Flow Cytometry using a BD LSRFortessa analyzer (BD Biosciences) or a Novocyte 3005 (ACEA, Agilent). Data were acquired using BD FACSDiva software or NovoExpress (Agilent) software respectively. The data were analyzed and FACS plots were generated using FlowJo (Treestar).

Cell enrichment & flow cytometry activated sorting

Splenocytes were lysed with ACK buffer (Life Technologies) to remove erythrocytes and were depleted for B cells using biotinylated anti-mouse

CD19 (clone: 6D5, RRID: AB_313639), any remaining blood cells using biotinylated anti-mouse TER119/ Erythroid cells (clone: TER119, RRID: AB_313705). Cells were stained with CD4 AF488 (clone: RM4-5, RRID: AB_389303), TCRβ PERCP/Cy5.5 (clone: H57-597, RRID: AB_1575173), CD25 APC (clone: PC61, RRID: AB_312861), aGalactosyl-Ceramide (aGal-Cer) loaded Tetramer PE. Live CD4⁺, CD25⁺, TCRβ⁺, tetramer- cells were sorted and used in downstream applications. Expanded cells in congenic recipients were sorted after staining with CD45.1 BV421 (clone: A20, RRID: AB_2562563) and CD45.2 PE (clone: 104, RRID: AB_313445) from Biolegend.

In all cases, dead cells were excluded using a fixable viability dye eFluor780 (eBioscience). The cells were sorted using an Aria Sorter (Becton Dickinson).

Adoptive transfer

For the first transplantations, we sorted CD4 cells from the spleen (as described) of *Tet2/3* DKO. Around 1-2 million cells were transferred by retroorbital injection to congenic, non-irradiated sex-matched, CD45.1⁺ recipients. Between 12-16 weeks post transfer mice were euthanized and organs were analyzed. For the secondary transplantations, 2 million CD45.2⁺ cells that had already expanded in CD45.1⁺ recipients were sorted and transferred by retroorbital injection to non-irradiated, congenic CD45.1⁺ recipients. Both male and female mice were analyzed with similar findings. For the serial transplantations shown in Figs. 5 and 7 500,000 cells were transferred. Mice were closely monitored since the expansion following the second transfer and the serial transplantations was faster. Mice were euthanized and analyzed 2 to 4 weeks post transfer. Male mice were analyzed.

Histology

Organs were isolated from mice immediately after euthanasia and were immersed in 10% Formalin (Fisher) for 48 h at room temperature. Then the samples were switched to 70% ethanol and processed in the UNC Lineberger Comprehensive Cancer Center (LCCC) Pathology Services Core. Paraffin embedded tissue blocks, sections and hematoxylin and eosin staining were prepared by the core. The sections were blindly evaluated by Dr. Stephanie Montgomery, a board-certified veterinary pathologist.

RNA sequencing (RNA-seq)

To analyze gene expression in peripheral CD4 cells, live CD4⁺ CD25⁻ TCRβ⁺, aGalCerCd1d tetramer- cells were sorted with purity of 98% or higher. To analyze gene expression in transplanted *Tet2/3* DKO CD4 cells, live, CD45.2⁺, CD45.1⁻ cells were sorted by Flow cytometry (purity >98%). RNA was isolated using the RNeasy Plus Mini Kit (Qiagen). RNA was quantified using Qubit High Sensitivity HS RNA kit (Invitrogen, catalogue number Q32852) in a Qubit 4 Fluorometer (Invitrogen). RNA integrity was assessed in a Bionalyzer (Agilent) using RNA 6000 pico kit (Agilent, catalogue number 5067-1513) or a TapeStation 4150 (Agilent) using Agilent High sensitivity RNA screen tape (Agilent, catalogue number: 5067-5579) and accompanying reagents such as high sensitivity RNA screen tape ladder (Agilent, catalogue number: 5067-5579) and high sensitivity RNA screen tape sample buffer (Agilent, catalogue number: 5067-5581). RNA with RIN value higher than 9 was used for library preparation. RNAseq library preparation and sequencing were performed by Beijing Genomics Institute (BGI).

Quantitative real-time PCR

Wild type or *Tet2/3* DKO live total CD4 cells (CD4⁺ CD25⁻ TCRβ⁺, aGalCerCd1d tetramer- cells as shown in Supplementary Figs. 1 and 2) were sorted with purity of at least 98%. RNA was isolated using Qiagen RNeasy plus Mini kit (catalogue number: 74134) or micro kit (catalogue number: 74034), depending on the number of the cells obtained by sorting. RNA quantification was performed with HS RNA kit (Invitrogen) in a Qubit 4 Fluorometer (Invitrogen). 100 ng of RNA were used to generate cDNA using the iScript Reverse Transcription SuperMix (Biorad, catalogue

number:1708840) following the instructions of the manufacturer. The generated cDNA was used to perform quantitative PCR with the iTaq Universal SYBR Green SuperMix (Biorad, catalogue number: 172-5121), on a CFX96 Real Time System (Biorad) using the following primers (purchased from IDT, with the exception of the primers for *Batf3* that were obtained from Biorad) for the indicated murine target genes:

Tet1^{18,19} Forward (Fwd): GAGCCTGTTCCCTCGATGTGG
Tet1 Reverse (Rvs): CAAACCCACCTGAGGCTGTT
Batf3 (Fwd & Rvs mix): PrimePCR SYBR Green Assay mouse *Batf3* (Biorad, Item: 10025636, concentration 20x)
*Irf4*⁷⁹ Fwd: AGATTCCAGGTGACTCTGTG
Irf4 Rvs: CTGCCCTGTCAGAGTATTTTC
*Hes1*⁸⁰ Fwd: CCAAGCTAGAGAAGGCAGACA
Hes1 Rvs: GTCACCTCGTTCATGCACCT
*Ki67*⁸¹ Fwd: TGCCCGACCCTACAAAATG
Ki67 Rvs: GAGCCTGTATCACTCATCTGTC
*Satb1*⁸² Fwd: CCCTCTAGGAAGAGGAAGGC
Satb1 Rvs: GTTCCACCACGCAGAAAATG
*Bcl11b*⁸¹ Fwd: AGGAGAGTATCTGAGCCAGTG
Bcl11b Rvs: GTTGTGCAAATGTAGCTGGAAG
*Lmo2*⁸³ Fwd: GAGGCGCTCTACTACAA
Lmo2 Rvs: GATCCGCTTGTCACAGGATG
Hprt Fwd⁸⁰: GGC CAG ACT TTG TTG GAT TTG
Hprt Rvs: CAC AGG ACT AGA ACA CCT GC

If the sequences of the primers have been previously reported, the reference is indicated after the target gene of interest.

Hprt primers were used for testing *Hprt* expression. Expression of the above target genes was normalized to *Hprt*. The comparative Ct method ($\Delta\Delta Ct$) was used to determine relative gene expression levels.

Whole genome sequencing

To assess chromosomal copy number, we performed whole genome sequencing. Genomic DNA was isolated from sorted wild type CD4 cells (Supplementary Fig. 2), sorted *Tet2/3* DKO CD4 T cells (from a young *Tet2/3* DKO mouse, 25 days old, Supplementary Fig. 1), or sorted expanded CD45.2+ *Tet2/3* DKO cells after one or two transplantations (Supplementary Fig. 4) in congenic CD45.1+ recipient mice using the PureLink genomic DNA mini kit (Invitrogen, catalogue number K182001). DNA was quantified (after dilution) using Qubit 1X dsDNA High Sensitivity (HS) (Invitrogen, catalogue number: Q33230) in a Qubit 4 fluorometer (Invitrogen). DNA was provided to the UNC HTSF and libraries were prepared using Illumina PCR free DNA library prep kit. Paired end, 2x 150 bp length sequencing was performed using Illumina NextSeq2000 P1 system. A summary of the samples that were sequenced and the reads acquired per sample is provided in Table 1.

Single-cell RNAseq library preparation: 10 x 3' v3.1 scRNA-seq experiment with TotalSeq-B hashtags

Spleens were harvested from male, 8 week-old CD45.1 recipients of CD45.2 *Tet2/3* DKO T cells after 2 days (3 replicates) and 10 days (3 replicates) post transfer. Splenocytes were dissociated and 2 million cells were stained with fixable viability dye (dilution 1:1000), anti-CD45.2 PE (clone: 104, RRID: AB_313445, Biolegend) and anti CD45.1-BV421 (clone: A20, RRID: AB_10896421, Biolegend). To allow multiplexing of cells, splenocytes from each condition were stained with TotalSeq antibodies (Biolegend) and were incubated for 30 min on ice. The TotalSeq antibodies used are summarized in Table 2.

Cells were washed 3 times to allow removal of excess antibodies. After sorting, CD45.1+ cells were provided to the UNC Advanced Analytical core for library preparation.

Cells were counted and viability was assessed using a Luna-FX7 automated cell counter (Logos biosystems). Briefly, cell viability was assessed and 5,000 per biological replicate and per condition were pooled yielding a total of 30,000 cells (15,000 for day 2 and 15,000 for day 10 post transfer). 10,000 cells were loaded in 10x Genomics Chromium Single Cell 3' inlets (three inlets in total were used). Single-cell gel beads in emulsion (GEM) were generated. Barcoding and library preparation were performed following manufacture instructions with the 10x Genomics Chromium Next GEM Single Cell 3' kit v3.1 (10X Genomics, Pleasanton, CA).

Libraries were sequenced on the Illumina NovaSeq at the UNC High Throughput Sequencing Facility Core. For hashtag library sequences, 88% antibody reads were mapped to cells. 2900 median genes per cell were identified after alignment to the reference genome.

Table 1 | Summary of samples for WGS

| Sample ID | Condition | Reads per sample |
|---|---------------------------------|------------------|
| WT splenic CD4 T cells mouse BR1 | Wild type | 17528898 |
| WT splenic CD4 T cells mouse BR2 | Wild type | 15896806 |
| WT splenic CD4 T cells mouse BR3 | Wild type | 15896806 |
| <i>Tet2/3</i> DKO splenic CD4 T cells (# B102_6, 25 days old) | Young <i>Tet2/3</i> DKO | 19942216 |
| <i>Tet2/3</i> expanded T cells (J3-2) | 1 st transplantation | 19109730 |
| <i>Tet2/3</i> expanded T cells (J3-3) | 1 st transplantation | 21172136 |
| <i>Tet2/3</i> expanded T cells (J4-5) | 1 st transplantation | 17721530 |
| <i>Tet2/3</i> expanded T cells (J3-6) | 2 nd transplantation | 23676074 |
| <i>Tet2/3</i> expanded T cells (J3-7) | 2 nd transplantation | 19455752 |
| <i>Tet2/3</i> expanded T cells (J22-3) | 2 nd transplantation | 25624438 |
| <i>Tet2/3</i> expanded T cells (J22-4) | 2 nd transplantation | 23758994 |

Table 2 | TotalSeq antibodies used for each sample

| Sample | # Ab product | # Ab barcode sequence |
|---|---|-----------------------|
| Biological replicate (BR1) 10 days (JAX 21) | TotalSeq-B0301 anti-mouse Hashtag 1 antibody RRID: AB_2814067, BioLegend Cat. No. 155831 | ACCCACCAGTAAGAC |
| BR2 10 days (JAX 22) | TotalSeq-B0302 anti-mouse Hashtag 2 antibody RRID: AB_2814068, BioLegend Cat. No. 155833 | GGTCGAGAGCATTCA |
| BR 3 10 days (JAX 25) | TotalSeq-B0303 anti-mouse Hashtag 3 antibody RRID: AB_2814069, BioLegend Cat. No. 155835 | CTTGCCGCATGTCAT |
| BR1 2 days (JAX 31) | TotalSeq-B0304 anti-mouse Hashtag 4 antibody RRID: AB_2814070, BioLegend Cat. No. 155837 | AAAGCATTCTTCACG |
| BR2 2 days (JAX 32) | TotalSeq-B0305 anti-mouse Hashtag 5 antibody RRID: AB_2814071, BioLegend Cat. No. 155839 | CTTTGCTTTGTGAG |
| BR3 2 days (JAX 33) | TotalSeq-B0306 anti-mouse Hashtag 6 antibody RRID: AB_2750037, BioLegend Cat. No. 155811 | TATGCTGCCACGGTA |

Statistics and reproducibility

Data were analyzed using Prism software (Graphpad). Unpaired student's *t* test was applied as indicated. In each figure legend, the indicated *P*-values are described. Data are mean ± s.e.m. In the graphs, each dot represents a mouse. Unless otherwise indicated the *P* value was not statistically significant (*P* > 0.05). Differences were considered significant when *p* < 0.05 (*); < 0.01 (**); < 0.001 (***) < 0.0001 (****).

For the phenotyping experiments, mice from different litters and of different sex were evaluated, with reproducible results. We used a minimum of three biological replicates.

For real-time qPCR experiments, we evaluated at least two biological replicates per gene. For most genes we assessed three biological replicates per gene.

In addition, we ensured that a minimum of 2 independent experiments was performed in each case. Statistical methods applied for bioinformatic analysis of large datasets are described in the relevant sections.

RNA-seq data analysis

Adapter trimming and quality filtering of the sequencing libraries was done using fastp (0.21.0)⁸⁴ with the default parameters. The sequencing libraries were mapped against mm10 and the GRCm38.100 transcriptome using STAR (2.7.5a)⁸⁵ with the following parameter values: --quantMode GeneCounts. The differential expression analysis was done using DESeq2⁸⁶ based on the read counts per gene produced by STAR. The used threshold for adjusted *p*-value was 0.01.

CMS-seq data analysis

The CMS-IP and input reads were mapped against mm10 using Bismark (0.22.3)⁸⁷. The mapping was done using the Bowtie 2 (2.4.5)⁸⁸ backend in the paired-end mode with the following parameter values: -I 0 -X 600 -N 0. The coverage tracks were generated using HOMER (4.10) (makeBigWig.pl -norm 1e6)⁸⁹ as we have previously described¹⁹. Profile plots were generated using deepTools⁹⁰ based on the GRCm38.100 gene models.

Whole genome sequencing data analysis

Adapter trimming and quality filtering of the sequencing libraries was done using fastp (0.21.0)⁸⁴ with the default parameters. The sequencing libraries were mapped against mm10 using Bowtie 2 (2.4.5)⁸⁸ (--very-sensitive -X 2000). The copy number variant detection was done using CNVkit (0.9.10)³⁹ from whole-genome sequencing data (cnvkit.py batch <SAMPLES> -n <CONTROL SAMPLES> -m wgs -f mm10.fa -d <OUTPUT-DIR> --scatter --diagram --annotate refFlat.txt).

Gene set enrichment analysis

Gene set enrichment analyses were done using GeneTrail 3⁹¹. The set of the LSK genes (*N* = 922) was taken from⁴⁰. The genes in the tested sets were ordered based on the log₂ fold-change either in ascending or decreasing order depending on the comparison.

Single-cell multiplexing data processing

Fastq files from each 10x Genomics library were pooled together and processed with the cellranger multi pipeline using Cell Ranger version 7.1.0. Mouse reference genome mm10-2020-A was used from 10x Genomics to align the reads. Given that there is no batch effect observed among libraries, the single-cell level gene count matrix from each library was then combined for all the downstream analysis.

Quality control, normalization, and clustering

Quality control, normalization and downstream analysis of single-cell level gene counts were performed using the Seurat R package (version 4, Satija Lab)⁹². A total number of 721 cells were removed from the downstream analysis if the total UMI count per cell is <500 or >100,000 or total number of detected genes is <200 or >6000 or the percent of reads mapped to mitochondrial genes is >10%. Log normalization was applied to each cell to control for the library size effect. Top 2000 genes were selected using the

“vst” method in Seurat. Principal component analysis was performed using the top 2000 genes and Louvain clustering was run using the first 30 PCs with resolution parameter 0.1.

Cell type annotation

Cell type annotation analysis was performed using R/SingleR⁹³ with the ImmGen ref. 43. Main labels from the ImmGen reference were used to assign cell label to each cell. To eliminate ambiguous cell type, we converted any cell type labels with less than 20 cells to “Others”. Each cluster was annotated by comparing the cell type annotation labels to the cluster labels derived using resolution parameter 0.1. Cd4 and Cd8 markers were used to identify CD4 T cells and CD8 T cells separately.

Differential expression and gene set enrichment analysis

Differential expression analysis was performed for each cell type of interest between the two time points using Pseudobulk method. First, the cell counts were aggregated across cells for each sample and then genes with less than 10 counts across all samples were removed. Differential expression analysis was performed using DESeq2⁸⁶ with Wald test and “parametric” fitType.

The Benjamini and Hochberg method was used to adjust the *p*-values and adjusted *p*-values < 0.05 was used to declare statistical significance.

Gene set enrichment analysis was performed using the R/fgsea package⁹⁴. The mouse hallmark gene sets from the Molecular Signatures Database (MSigDB)^{95–97} were used. For the Wilcoxon method, all genes were ranked by average log₂FC and used as input when running the fgsea() function. For the pseudobulk method, all genes were ranked by the Wald test statistic and used as input when running the fgsea() function. Adjusted *p*-value threshold of 0.05 was used to call statistical significance.

Reporting summary

Further information on research design is available in the Nature Portfolio Reporting Summary linked to this article.

Data availability

Bulk RNA-seq and WGS datasets have been deposited in the Gene Expression Omnibus (GEO) public repository under the accession code GSE279236. Single cell RNA-seq datasets have been deposited in the GEO public repository under the accession code GSE278239. We have not generated unique or novel codes for data analysis for this manuscript. We have provided a detailed data analysis section. Most of the biological tools (mouse strains) are available at Jackson laboratories and we have provided the relevant stock numbers. The source data for all figures are provided in Supplementary Data 3. All other data are available from the corresponding author on reasonable request.

Received: 9 April 2024; Accepted: 22 November 2024;

Published online: 03 December 2024

References

1. Tahiliani, M. et al. Conversion of 5-methylcytosine to 5-hydroxymethylcytosine in mammalian DNA by MLL partner TET1. *Science* **324**, 930–935 (2009).
2. Ito, S. et al. Tet proteins can convert 5-methylcytosine to 5-formylcytosine and 5-carboxylcytosine. *Science* **333**, 1300–1303 (2011).
3. Ko, M. et al. Impaired hydroxylation of 5-methylcytosine in myeloid cancers with mutant TET2. *Nature* **468**, 839–843 (2010).
4. Delhommeau, F. et al. Mutation in TET2 in myeloid cancers. *N. Engl. J. Med.* **360**, 2289–2301 (2009).
5. Langemeijer, S. M. et al. Acquired mutations in TET2 are common in myelodysplastic syndromes. *Nat. Genet.* **41**, 838–842 (2009).
6. Tsiouplis, N. J., Bailey, D. W., Chiou, L. F., Wissink, F. J. & Tsagaratou, A. TET-Mediated Epigenetic Regulation in Immune Cell Development and Disease. *Front. Cell Dev. Biol.* **8**, 623948 (2020).

7. Sakata-Yanagimoto, M. et al. Somatic RHOA mutation in angioimmunoblastic T cell lymphoma. *Nat. Genet.* **46**, 171–175 (2014).
8. Quivoron, C. et al. TET2 inactivation results in pleiotropic hematopoietic abnormalities in mouse and is a recurrent event during human lymphomagenesis. *Cancer Cell* **20**, 25–38 (2011).
9. Palomero, T. et al. Recurrent mutations in epigenetic regulators, RHOA and FYN kinase in peripheral T cell lymphomas. *Nat. Genet.* **46**, 166–170 (2014).
10. Cortes, J. R. & Palomero, T. Biology and Molecular Pathogenesis of Mature T-Cell Lymphomas. *Cold Spring Harb. Perspect. Med.* <https://doi.org/10.1101/cshperspect.a035402> (2020).
11. Ko, M. et al. Ten-Eleven-Translocation 2 (TET2) negatively regulates homeostasis and differentiation of hematopoietic stem cells in mice. *Proc. Natl Acad. Sci. USA* **108**, 14566–14571 (2011).
12. Moran-Crusio, K. et al. Tet2 loss leads to increased hematopoietic stem cell self-renewal and myeloid transformation. *Cancer Cell* **20**, 11–24 (2011).
13. Ito, K. et al. Non-catalytic Roles of Tet2 Are Essential to Regulate Hematopoietic Stem and Progenitor Cell Homeostasis. *Cell Rep.* **28**, 2480–2490.e2484 (2019).
14. Yeaton, A. et al. The impact of inflammation-induced tumor plasticity during myeloid transformation. *Cancer Discov.* <https://doi.org/10.1158/2159-8290.CD-21-1146> (2022).
15. Cortes, J. R. et al. RHOA G17V Induces T Follicular Helper Cell Specification and Promotes Lymphomagenesis. *Cancer Cell* **33**, 259–273.e257 (2018).
16. Tsagaratou, A. et al. Dissecting the dynamic changes of 5-hydroxymethylcytosine in T-cell development and differentiation. *Proc. Natl Acad. Sci. USA* **111**, E3306–E3315 (2014).
17. Theofilatos, D. et al. Deciphering the TET3 interactome in primary thymic developing T cells. *iScience* **27**, 109782 (2024).
18. Tsagaratou, A. et al. TET proteins regulate the lineage specification and TCR-mediated expansion of iNKT cells. *Nat. Immunol.* **18**, 45–53 (2017).
19. Aijo, T. et al. TET proteins regulate T cell and iNKT cell lineage specification in a TET2 catalytic dependent manner. *Front. Immunol.* **13**, 940995 (2022).
20. Gioulbasani, M., Åijö, T., Valenzuela, J. E., Buquera Bettes, J. & Tsagaratou, A. TET proteins regulate Drosha expression and impact microRNAs in iNKT cells. *Front Immunol.* **15**, 1440044 (2024).
21. Pobezinsky, L. A. et al. Let-7 microRNAs target the lineage-specific transcription factor PLZF to regulate terminal NKT cell differentiation and effector function. *Nat. Immunol.* **16**, 517–524 (2015).
22. Yue, X. et al. Control of Foxp3 stability through modulation of TET activity. *J. Exp. Med.* **213**, 377–397 (2016).
23. Yang, R. et al. Hydrogen Sulfide Promotes Tet1- and Tet2-Mediated Foxp3 Demethylation to Drive Regulatory T Cell Differentiation and Maintain Immune Homeostasis. *Immunity* **43**, 251–263 (2015).
24. Nair, V. S., Song, M. H., Ko, M. & Oh, K. I. DNA Demethylation of the Foxp3 Enhancer Is Maintained through Modulation of Ten-Eleven-Translocation and DNA Methyltransferases. *Mol. Cells* **39**, 888–897 (2016).
25. Bendelac, A., Savage, P. B. & Teyton, L. The biology of NKT cells. *Annu Rev. Immunol.* **25**, 297–336 (2007).
26. Yue, X., Lio, C. J., Samaniego-Castruita, D., Li, X. & Rao, A. Loss of TET2 and TET3 in regulatory T cells unleashes effector function. *Nat. Commun.* **10**, 2011 (2019).
27. Cimmino, L. et al. TET1 is a tumor suppressor of hematopoietic malignancy. *Nat. Immunol.* **16**, 653–662 (2015).
28. An, J. et al. Acute loss of TET function results in aggressive myeloid cancer in mice. *Nat. Commun.* **6**, 10071 (2015).
29. Schnell, S. A. et al. Therapeutic targeting of HES1 transcriptional programs in T-ALL. *Blood* **125**, 2806–2814 (2015).
30. Espinosa, L. et al. The Notch/Hes1 pathway sustains NF-kappaB activation through CYLD repression in T cell leukemia. *Cancer Cell* **18**, 268–281 (2010).
31. Nakagawa, M. et al. Targeting the HTLV-I-Regulated BATF3/IRF4 Transcriptional Network in Adult T Cell Leukemia/Lymphoma. *Cancer Cell* **34**, 286–297.e210 (2018).
32. Huang, Y. et al. The behaviour of 5-hydroxymethylcytosine in bisulfite sequencing. *PLoS One* **5**, e8888 (2010).
33. Huang, Y., Pastor, W. A., Zepeda-Martinez, J. A. & Rao, A. The anti-CMS technique for genome-wide mapping of 5-hydroxymethylcytosine. *Nat. Protoc.* **7**, 1897–1908 (2012).
34. Pastor, W. A. et al. Genome-wide mapping of 5-hydroxymethylcytosine in embryonic stem cells. *Nature* **473**, 394–397 (2011).
35. Yue, X. et al. Whole-genome analysis of TET dioxygenase function in regulatory T cells. *EMBO Rep.* **22**, e52716 (2021).
36. Ichiyama, K. et al. The methylcytosine dioxygenase Tet2 promotes DNA demethylation and activation of cytokine gene expression in T cells. *Immunity* **42**, 613–626 (2015).
37. Tsagaratou, A. TET Proteins in the Spotlight: Emerging Concepts of Epigenetic Regulation in T Cell Biology. *Immunohorizons* **7**, 106–115 (2023).
38. Lollies, A. et al. An oncogenic axis of STAT-mediated BATF3 upregulation causing MYC activity in classical Hodgkin lymphoma and anaplastic large cell lymphoma. *Leukemia* **32**, 92–101 (2018).
39. Talevich, E., Shain, A. H., Botton, T. & Bastian, B. C. CNVkit: Genome-Wide Copy Number Detection and Visualization from Targeted DNA Sequencing. *PLoS Comput. Biol.* **12**, e1004873 (2016).
40. Li, J. et al. ZMYND11-MBTD1 induces leukemogenesis through hijacking NuA4/TIP60 acetyltransferase complex and a PWWP-mediated chromatin association mechanism. *Nat. Commun.* **12**, 1045 (2021).
41. Issuree, P. D. et al. Stage-specific epigenetic regulation of CD4 expression by coordinated enhancer elements during T cell development. *Nat. Commun.* **9**, 3594 (2018).
42. Zheng, W. & Flavell, R. A. The transcription factor GATA-3 is necessary and sufficient for Th2 cytokine gene expression in CD4 T cells. *Cell* **89**, 587–596 (1997).
43. Heng, T. S., Painter, M. W. & Immunological Genome Project, C. The Immunological Genome Project: networks of gene expression in immune cells. *Nat. Immunol.* **9**, 1091–1094 (2008).
44. Habib, T. et al. Myc stimulates B lymphocyte differentiation and amplifies calcium signaling. *J. Cell Biol.* **179**, 717–731 (2007).
45. de Alboran, I. M. et al. Analysis of C-MYC function in normal cells via conditional gene-targeted mutation. *Immunity* **14**, 45–55 (2001).
46. Calado, D. P. et al. The cell-cycle regulator c-Myc is essential for the formation and maintenance of germinal centers. *Nat. Immunol.* **13**, 1092–1100 (2012).
47. Perez-Olivares, M. et al. Functional interplay between c-Myc and Max in B lymphocyte differentiation. *EMBO Rep.* **19**, <https://doi.org/10.15252/embr.201845770> (2018).
48. Kieffer-Kwon, K. R. et al. Myc Regulates Chromatin Decompaction and Nuclear Architecture during B Cell Activation. *Mol. Cell* **67**, 566–578.e510 (2017).
49. Braun, D., Caramalho, I. & Demengeot, J. IFN-alpha/beta enhances BCR-dependent B cell responses. *Int. Immunol.* **14**, 411–419 (2002).
50. Zhao, Z. et al. Combined Loss of Tet1 and Tet2 Promotes B Cell, but Not Myeloid Malignancies, in Mice. *Cell Rep.* **13**, 1692–1704 (2015).
51. Georges, R. O. et al. Acute deletion of TET enzymes results in aneuploidy in mouse embryonic stem cells through decreased expression of Khdc3. *Nat. Commun.* **13**, 6230 (2022).
52. Kafer, G. R. et al. 5-Hydroxymethylcytosine Marks Sites of DNA Damage and Promotes Genome Stability. *Cell Rep.* **14**, 1283–1292 (2016).

53. Iurlaro, M. et al. A screen for hydroxymethylcytosine and formylcytosine binding proteins suggests functions in transcription and chromatin regulation. *Genome Biol.* **14**, R119 (2013).
54. Spruijt, C. G. et al. Dynamic readers for 5-(hydroxy)methylcytosine and its oxidized derivatives. *Cell* **152**, 1146–1159 (2013).
55. Lopez-Moyado, I. F. et al. Paradoxical association of TET loss of function with genome-wide DNA hypomethylation. *Proc. Natl Acad. Sci. USA* **116**, 16933–16942 (2019).
56. Fraietta, J. A. et al. Disruption of TET2 promotes the therapeutic efficacy of CD19-targeted T cells. *Nature* **558**, 307–312 (2018).
57. Carty, S. A. et al. The Loss of TET2 Promotes CD8(+) T Cell Memory Differentiation. *J. Immunol.* **200**, 82–91 (2018).
58. Dong, C. Cytokine Regulation and Function in T Cells. *Annu Rev. Immunol.* **39**, 51–76 (2021).
59. Choi, J. et al. Bcl-6 is the nexus transcription factor of T follicular helper cells via repressor-of-repressor circuits. *Nat. Immunol.* **21**, 777–789 (2020).
60. Choi, J. & Crotty, S. Bcl6-Mediated Transcriptional Regulation of Follicular Helper T cells (TFH). *Trends Immunol.* **42**, 336–349 (2021).
61. Iqbal, J. et al. Gene expression signatures delineate biological and prognostic subgroups in peripheral T-cell lymphoma. *Blood* **123**, 2915–2923 (2014).
62. Heavican, T. B. et al. Genetic drivers of oncogenic pathways in molecular subgroups of peripheral T-cell lymphoma. *Blood* **133**, 1664–1676 (2019).
63. Tsagaratou, A. Deciphering the multifaceted roles of TET proteins in T-cell lineage specification and malignant transformation. *Immunol. Rev.* **300**, 22–36 (2021).
64. Cismasiu, V. B. et al. BCL11B functionally associates with the NuRD complex in T lymphocytes to repress targeted promoter. *Oncogene* **24**, 6753–6764 (2005).
65. Hosokawa, H. et al. Bcl11b sets pro-T cell fate by site-specific cofactor recruitment and by repressing *Id2* and *Zbtb16*. *Nat. Immunol.* **19**, 1427–1440 (2018).
66. Hu, G. et al. Transformation of Accessible Chromatin and 3D Nucleome Underlies Lineage Commitment of Early T Cells. *Immunity* **48**, 227–242.e228 (2018).
67. Zelenka, T. et al. The 3D enhancer network of the developing T cell genome is shaped by SATB1. *Nat. Commun.* **13**, 6954 (2022).
68. Papadogkonas, G., Papamatheakis, D. A. & Spilianakis, C. 3D Genome Organization as an Epigenetic Determinant of Transcription Regulation in T Cells. *Front. Immunol.* **13**, 921375 (2022).
69. Feng, D. et al. Chromatin organizer SATB1 controls the cell identity of CD4(+) CD8(+) double-positive thymocytes by regulating the activity of super-enhancers. *Nat. Commun.* **13**, 5554 (2022).
70. Wang, B., Ji, L. & Bian, Q. SATB1 regulates 3D genome architecture in T cells by constraining chromatin interactions surrounding CTCF-binding sites. *Cell Rep.* **42**, 112323 (2023).
71. Cimmino, L. & Aifantis, I. Alternative roles for oxidized mCs and TETs. *Curr. Opin. Genet. Dev.* **42**, 1–7 (2017).
72. Ziller, M. J. et al. Charting a dynamic DNA methylation landscape of the human genome. *Nature* **500**, 477–481 (2013).
73. Smith, Z. D., Hetzel, S. & Meissner, A. DNA methylation in mammalian development and disease. *Nat Rev Genet.* <https://doi.org/10.1038/s41576-024-00760-8> (2024).
74. Guillaumot, M., Cimmino, L. & Aifantis, I. The Impact of DNA Methylation in Hematopoietic Malignancies. *Trends Cancer* **2**, 70–83 (2016).
75. Nestor, C. E. et al. Rapid reprogramming of epigenetic and transcriptional profiles in mammalian culture systems. *Genome Biol.* **16**, 11 (2015).
76. Ko, M. et al. TET proteins and 5-methylcytosine oxidation in hematological cancers. *Immunol. Rev.* **263**, 6–21 (2015).
77. Kang, J. et al. Simultaneous deletion of the methylcytosine oxidases Tet1 and Tet3 increases transcriptome variability in early embryogenesis. *Proc. Natl Acad. Sci. USA* **112**, E4236–E4245 (2015).
78. Gioulbasani, M. & Tsagaratou, A. Defining iNKT Cell Subsets and Their Function by Flow Cytometry. *Curr. Protoc.* **3**, e838 (2023).
79. Williams, J. W. et al. Transcription factor IRF4 drives dendritic cells to promote Th2 differentiation. *Nat. Commun.* **4**, 2990 (2013).
80. Tremblay, M. et al. Modeling T-cell acute lymphoblastic leukemia induced by the SCL and LMO1 oncogenes. *Genes Dev.* **24**, 1093–1105 (2010).
81. Cai, S. et al. A Quiescent Bcl11b High Stem Cell Population Is Required for Maintenance of the Mammary Gland. *Cell Stem Cell* **20**, 247–260.e245 (2017).
82. Nomura, A. et al. Identification of a novel enhancer essential for *Satb1* expression in T(H)2 cells and activated ILC2s. *Life Sci Alliance* **6**, <https://doi.org/10.26508/lsa.202301897> (2023).
83. Hirano, K. I. et al. LMO2 is essential to maintain the ability of progenitors to differentiate into T-cell lineage in mice. *Elife* **10**, <https://doi.org/10.7554/eLife.68227> (2021).
84. Chen, S., Zhou, Y., Chen, Y. & Gu, J. fastp: an ultra-fast all-in-one FASTQ preprocessor. *Bioinformatics* **34**, i884–i890 (2018).
85. Dobin, A. et al. STAR: ultrafast universal RNA-seq aligner. *Bioinformatics* **29**, 15–21 (2013).
86. Love, M. I., Huber, W. & Anders, S. Moderated estimation of fold change and dispersion for RNA-seq data with DESeq2. *Genome Biol.* **15**, 550 (2014).
87. Krueger, F. & Andrews, S. R. Bismark: a flexible aligner and methylation caller for Bisulfite-Seq applications. *Bioinformatics* **27**, 1571–1572 (2011).
88. Langmead, B. & Salzberg, S. L. Fast gapped-read alignment with Bowtie 2. *Nat. Methods* **9**, 357–359 (2012).
89. Heinz, S. et al. Simple combinations of lineage-determining transcription factors prime cis-regulatory elements required for macrophage and B cell identities. *Mol. Cell* **38**, 576–589 (2010).
90. Ramirez, F. et al. deepTools2: a next generation web server for deep-sequencing data analysis. *Nucleic Acids Res.* **44**, W160–W165 (2016).
91. Gerstner, N. et al. GeneTrail 3: advanced high-throughput enrichment analysis. *Nucleic Acids Res.* **48**, W515–W520 (2020).
92. Hao, Y. et al. Integrated analysis of multimodal single-cell data. *Cell* **184**, 3573–3587.e3529 (2021).
93. Aran, D. et al. Reference-based analysis of lung single-cell sequencing reveals a transitional profibrotic macrophage. *Nat. Immunol.* **20**, 163–172 (2019).
94. Korotkevich, G. et al. Fast gene set enrichment analysis. *bioRxiv*, 060012, <https://doi.org/10.1101/060012> (2021).
95. Subramanian, A. et al. Gene set enrichment analysis: a knowledge-based approach for interpreting genome-wide expression profiles. *Proc. Natl Acad. Sci. USA* **102**, 15545–15550 (2005).
96. Liberzon, A. et al. The Molecular Signatures Database (MSigDB) hallmark gene set collection. *Cell Syst.* **1**, 417–425 (2015).
97. Castanza, A. S. et al. Extending support for mouse data in the Molecular Signatures Database (MSigDB). *Nat. Methods* **20**, 1619–1620 (2023).

Acknowledgements

We wish to thank Ms. Kayla Harrison and Ms. Theresa Hegarty (UNC DCM Colony Management Core) for excellent mouse colony management. We acknowledge Ms. Janet Dow and Ms. Ayrianna Woody of the UNC Flow Cytometry Core for their expert help with FACS sorting. Research reported in this publication and related to FACS sorting was supported in part by the North Carolina Biotech Center Institutional Support Grant 2012-IDG-1006. We wish to thank Mr. Mark Ross from the UNC Preclinical Research Unit for his expert assistance with retroorbital injections and unbiased monitoring of mice during the initial phase of the study. We wish to acknowledge the UNC Pathology Services Core for sections and histopathology analysis. The UNC High Throughput Sequencing core (HTSF) for sequencing. The above cores affiliated to UNC Lineberger Comprehensive Cancer Center are supported in

part by P30 CA016086 Cancer Center Core Support Grant to the UNC Lineberger Comprehensive Cancer Center. The 10x Genomics Single-Cell RNA-seq library preparation was performed by Ms. Gabrielle Canon of the UNC Center of Gastrointestinal Biology and Disease (CGIBD) Advanced Analytics Core (AAC). CGIBD AAC is supported by NIH grant P30 DK034987. We thank Mr. Carlton Anderson of the UNC AAC and Mr. Hank Beggs (Biolegend) for advice regarding cell hashing for the single cell RNA-seq experiments, using TotalSeq antibodies. We thank Matt Soloway at the UNC Lineberger Bioinformatics core for assistance with depositing single-cell RNA-seq data at GEO. We thank the Duke University School of Medicine for the use of Sequencing and Genomic Technologies Shared Resource, which provided sequencing services. We gratefully acknowledge the NIH tetramer core for generously providing aGalactosyl-Ceramide loaded mouse CD1d tetramers. This work was supported by NIH grant (R35-GM138289), Supplement 3R35-GM138289-02S1 from National Institute of General Medicinal Sciences (NIGMS), and UNC Lineberger Comprehensive Cancer Center Startup funds (to A.T.).

Author contributions

M.G. performed cell isolation, flow cytometry and adoptive transfer experiments, isolated RNA, performed quantitative PCR experiments, prepared samples for single cell RNA sequencing and contributed in data analysis and interpretation. T.Ä. analyzed all the bulk genome-wide sequencing datasets, generated the related figures, interpreted data and wrote the genome wide data analysis methods section. S.L. analyzed the single cell RNA-seq data, generated the relevant figures and wrote the related data analysis section. S.M. blindly evaluated histology sections and took images. N.M. additionally assessed histological samples. D.C. supervised the single-cell RNA-seq data analysis. A.T. conceived and supervised the study, designed, performed and analyzed experiments, secured funding and wrote the manuscript with input from all the authors. All authors agree to the content of the manuscript.

Competing interests

T.Ä. is a Director of Data Science at Covera Health. No funding from Covera Health was provided for this work. The other authors have no conflict of interest to declare.

Additional information

Supplementary information The online version contains supplementary material available at <https://doi.org/10.1038/s42003-024-07312-0>.

Correspondence and requests for materials should be addressed to Ageliki Tsagaratou.

Peer review information *Communications Biology* thanks the anonymous reviewers for their contribution to the peer review of this work. Primary Handling Editors: Guideng Li and Dario Ummarino.

Reprints and permissions information is available at <http://www.nature.com/reprints>

Publisher's note Springer Nature remains neutral with regard to jurisdictional claims in published maps and institutional affiliations.

Open Access This article is licensed under a Creative Commons Attribution-NonCommercial-NoDerivatives 4.0 International License, which permits any non-commercial use, sharing, distribution and reproduction in any medium or format, as long as you give appropriate credit to the original author(s) and the source, provide a link to the Creative Commons licence, and indicate if you modified the licensed material. You do not have permission under this licence to share adapted material derived from this article or parts of it. The images or other third party material in this article are included in the article's Creative Commons licence, unless indicated otherwise in a credit line to the material. If material is not included in the article's Creative Commons licence and your intended use is not permitted by statutory regulation or exceeds the permitted use, you will need to obtain permission directly from the copyright holder. To view a copy of this licence, visit <http://creativecommons.org/licenses/by-nc-nd/4.0/>.

© The Author(s) 2024